Effect of acute and chronic aldosterone exposure on the retinal pigment epithelium-choroid complex in rodents

Jérémie Canonica, Chadi Mehanna, Benjamin Bonnard, Laurent Jonet, Emmanuelle Gelize, Jean-Philippe Jais, Frederic Jaisser, Min Zhao, Francine Behar-Cohen

Effect of acute and chronic aldosterone exposure on the retinal pigment epithelium-choroid complex in rodents

Jérémie Canonica[1, 2]*, Chadi Mehanna[3, 4]*, Benjamin Bonnard[5], Laurent Jonet[1], Emmanuelle Gelize[1], Jean-Philippe Jais[4], Frederic Jaisser[5], Min Zhao[1], Francine Behar-Cohen[1, 3]

[1]INSERM, UMRS 1138, Team 17, Centre de Recherche des Cordeliers, Sorbonne University, Paris Descartes University, 75006 Paris, France

[2] Department of Ophthalmology, University of Lausanne, Switzerland

[3] Department of Ophthalmology, Ophthalmopole, Hôpital Cochin, Assistance Publique - Hôpitaux de Paris, 75014 Paris, France

[4] Department of Biostatistics, Hôpital Necker-EnfantsMalades, AP-HP, 75015 Paris, France

[5] INSERM, UMRS 1138, Team 17, Centre de Recherche des Cordeliers, Sorbonne University, Paris Descartes University, 75006 Paris, France

* Jérémie Canonica and Chadi Mehanna contributed equally to this work.

Corresponding author:
Francine Behar-Cohen
Centre de Recherche des Cordeliers
15 rue de l'Ecole de Médecine 75006 Paris
Francine.behar@gmail.com

Highlights

- Acute intravitreous administration of high dose aldosterone leads to retinal inflammation and induces in the rat RPE-choroid complex, the expression of genes involved in the inflammatory response, oxidative stress, extracellular remodeling, synaptic activity and muscle contraction, cellular metabolism and transports, cytoskeleton and cell junctions, and necroptosis.
- In the NAS mouse model, systemic chronic aldosterone/salt exposure induces retinal edema, RPE phagocytosis dysfunction and choroidal vasodilation. Genes involved in inflammation, oxidative stress, angiogenesis and cell contractility and migration are deregulated in the RPE-choroid complex of NAS mice.

- These two rodent models of acute and chronic aldosterone exposure share some common phenotypic and molecular features at the RPE-choroid complex level, that could contribute to pachychoroid epitheliopathy in humans.

Keywords: mineralocorticoid receptor, inflammation, RNA sequencing, retina

Abstract

Preclinical and clinical evidences show that aldosterone and/or mineralocorticoid receptor (MR) over-activation by glucocorticoids can be deleterious to the retina and to the retinal pigment epithelium (RPE)-choroid complex. However, the exact molecular mechanisms driving these effects remain poorly understood and pathological consequences of chronic exposure of the retina and RPE/ choroid to aldosterone have not been completely explored. We aimed to decipher the transcriptomic regulation in the RPE-choroid complex in rats in response to acute intraocular aldosterone injection and to explore the consequences of systemic chronic aldosterone exposure on the morphology and the gene regulation in RPE/ choroid in mice. High dose of aldosterone (100 nM) was intravitreously injected in Lewis rat eyes in order to yield an aldosterone dose able to induce a molecular response at the apical side of the RPE-choroid complex. The posterior segment morphology was evaluated *in vivo* using optical coherence tomography (OCT) before and 24 hours after aldosterone injection. Rat RPE-choroid complexes were used for RNA sequencing and analysis. Uninephrectomy/aldosterone/salt (NAS) model was created in wild-type C57BL/6 mice. After 6 weeks, histology of mouse posterior segments were observed *ex vivo*. Gene expression in the RPE-choroid complex was analyzed using quantitative PCR. Acute intravitreous injection of aldosterone induced posterior segment inflammation observed on OCT. RNA sequencing of rat RPE-choroid complexes revealed up-regulation of pathways involved in inflammation, oxidative stress and RNA procession, and down-regulation of genes involved in synaptic activity, muscle contraction, cytoskeleton, cell junction and transporters. Chronic aldosterone/salt exposure in NAS model induces retinal edema, choroidal vasodilation and RPE cell dysfunction and migration. Quantitative PCR showed deregulation of genes involved in inflammatory response, oxidative stress, particularly the NOX pathway, angiogenesis and cell contractility. Both rodent models share some common phenotypes and molecular regulations in the RPE-choroid complex that could contribute to pachychoroid epitheliopathy in humans. The difference in inflammatory status relies on different intraocular or systemic route of aldosterone administration and on the different doses of aldosterone exposed to the RPE-choroid complex.

1. Introduction

Aldosterone is produced and secreted by the adrenal gland in response to the renin-angiotensin system stimulation, described as the renin-angiotensin-aldosterone system (RAAS) (Lumbers, 1999; Peters, 2012). Upon aldosterone binding to the mineralocorticoid receptor (MR), a member of the steroid receptor family expressed in kidney epithelial cells, expression of genes involved in sodium retention regulating body aqueous volume and blood pressure is induced. MR is activated by both aldosterone and cortisol, that largely prevailed in the circulation and occupy MR in most cells and organs (Lan et al., 1982). In cells expressing the 11beta-hydroxysteroid dehydrogenase type 2 enzyme (HSD2), which metabolizes cortisol or corticosterone into inactive metabolites with low affinity for MR and for the glucocorticoid receptor (GR), aldosterone exerts specific effects through MR binding (Matulich et al., 1976). Transcriptional regulations resulting from GR and MR activation are highly dose and cell dependent (Lim-Tio et al., 1997).

Preclinical and clinical studies demonstrated significant beneficial renal, cardiac and vascular effects of mineralocorticoid receptor antagonists (MRA) at doses that induced only small reductions in blood pressure, suggesting that MR activation exerts direct deleterious effects in various organs (Kolkhof and Bärfacker, 2017). MR has been shown to be expressed in vascular endothelial cells and in smooth muscle cells (Chrissobolis, 2017) and aldosterone excess or MR over-activation induces oxidative stress, endothelial dysfunction, inflammation, vascular remodeling, stiffening, and fibrosis (Biwer et al., 2019).

As shown in the brain (Brooke et al., 1994), MR is also expressed in the neural retina (Golestaneh et al., 2002), in the retinal pigment epithelium (RPE) and in the choroid vasculature (Zhao et al., 2010, 2012), but whether aldosterone freely diffuses from the circulation into the eye is unknown. The retina being part of the central nervous system, it is plausible that similarly to the brain, control of steroid entry by efflux transporters is active (Hindle et al., 2017). Noticeably, in the brain, MR is mostly occupied by glucocorticoids in physiological conditions (De Kloet et al., 1998). Acute intraocular injection of low aldosterone dose induced the expression and mislocalization of Kir 4.1 and AQP4 channels in retinal glial Müller cells (Zhao et al., 2010) and provoked retinal edema. In addition, it induced choroidal vasodilation (Zhao et al., 2012) due to, at least in part, to the expression of Kca2.3 channel in vascular endothelial cells located in the choroidal vasculature but not in the retinal vasculature (Zhao et al., 2012). Upon repeated aldosterone intraocular injections, subretinal fluid accumulated, mimicking the features of Central Serous ChorioRetinopathy

(CSCR) (Zhao et al., 2012). Based on these observations, it was suggested that MR pathway over-activation could contribute to CSCR, since intake of glucocorticoids, that also bind to MR, is a known risk factor for CSCR (Nicholson et al., 2018). In addition, patients with hyperaldosteronism also showed features of CSCR (van Dijk et al., 2016) and genetic polymorphism in *NR3C2*, gene encoding MR, was associated with an increased risk for CSCR (van Dijk et al., 2017). More recently, we showed that MR activation was involved in choroidal neovascularization in rodents and that MRA exerted beneficial anti-edematous effects in patients with neovascular age-related macular degeneration, resistant to anti-VEGF (Zhao et al., 2019). The pro-angiogenic effects of aldosterone on the retina was also demonstrated in the rodent model of retinopathy of prematurity (Wilkinson-Berka et al., 2009). In addition, aldosterone aggravated the retinal edema induced by retinal vein occlusion in rodents through impaired drainage mechanisms by retinal glial Müller cells and through the enhancement of monocytes retinal infiltration (Allingham et al., 2018).

Thus, preclinical and clinical evidences show that aldosterone and/or MR over-activation by glucocorticoids excess or spontaneously, can be deleterious to the retina and to the RPE-choroid complex. However, the exact molecular mechanisms driving these effects remain poorly understood and pathological consequences of chronic exposure of the retina to aldosterone have not been completely explored.

The aims of this work were: (*i*) to decipher the transcriptomic regulation in the RPE-choroid complex in rats in response to acute intraocular aldosterone injection and, (*ii*) to explore the consequences of systemic chronic aldosterone exposure on the RPE/choroid and retina in mice.

2. Material and methods

2.1. Animals

All experiments were performed in accordance with the European Communities Council Directive 86/609/EEC and French national regulations and approved by local ethical committees (#4488 and #2541, Charles Darwin). Animals were kept in pathogen-free conditions with food, water and litter, and housed in a 12-hour/12-hour light/dark cycle.

2.2. Intravitreous injection of aldosterone in rat eyes and retinal morphology

Eight-week old male Lewis rats were anesthetized by intramuscular injection of ketamine (40 mg/kg) and Xylazine (4 mg/kg). Intravitreous injections (IVT) were performed using microfine (300 µL) syringes with 31G needles under topical anesthesia (tetracaine 1%,

Aldrich, Lyon, France). Rat eyes were injected with 5 µL aldosterone diluted in 0.9% saline to obtain a concentration of 1 µM for injection, corresponding to a final concentration of 100 nM in the vitreous. Since no more than 10% of steroids injected into the vitreous is expected to reach the retina (Chang-Lin et al., 2011), we estimated the concentration of aldosterone at about 10 nM that reach the RPE-choroid complex level, which is a specific dose to evaluate aldosterone effects. Control rat eyes were injected with 5 µL saline. Both eyes of 6 rats per group were injected.

Retinal morphology was assessed *in vivo* on anesthetized rats using Micron III Image-guided optical coherence tomography (OCT, Phoenix Research Labs, Pleasanton, CA, USA). Pupils were dilated with drops of Mydriaticum (2mg/0.4 mL, VIDAL, Issy Les Moulineaux, France). OCT scan location was presented on a bright-field retinal image, and OCT real-time images of the retinal cross sections were taken with Micron OCT software. The bright-field retinal images were also captured simultaneously using StreamPix software. OCT images of the same retinal location were compared before and 24 hours after IVT.

2.3. RNA-sequencing of rat RPE-choroid complex and data analysis

Rats were sacrificed 24 hours after IVT, the eyes were enucleated and the RPE-choroid complexes were dissected. Total RNA was extracted using a Precellys Homogenizer (Ozyme, Bertin) and an RNeasy Mini Kit (Qiagen, Courtaboeuf, France) and treated with DNase I (Qiagen). RNA of both eyes from the same animal was pooled for RNA sequencing. Samples were sent for sequencing at the iGenSeq transcriptomic platform of the Brain and Spine Institute (ICM, Paris, France). RNA quality was checked by capillary electrophoresis (Agilent 2100 Bioanalyzer system) and RNA with integrity numbers (RIN) ranging from 7.8 to 8.2 was accepted for library generation. The cDNA library of each sample was prepared with a KAPA mRNA Hyper Prep (Roche) for 75 bp paired-end reads, according to the manufacturer's instructions. Each of the cDNA libraries was indexed for multiplexing (2x60 million reads/sample), and indexed libraries were sequenced on one lane of the Illumina Nextseq 500 device. Data were recorded in the FASTQ format. For the differential gene expression (DGE), gene enrichment and gene ontology (GO) analyses, R version 3.5.0 (R Core Team (2018)) and RStudio version 1.1.447 were used. After loading of the data and addition of the Rattus norvegicus annotations, a filtering excluded the genes which are not expressed. Standardization was made using TMM (trimmed mean of M-values) present in the package edgeR-robust. After estimating the dispersion parameter of the negative binomial distribution, the generalized linear model was fitted with a maximum of quasi-likelihood to

take into account the uncertainty in the estimation of the dispersion parameter and to increase the robustness. After the fit of the model, the differential expression of the genes was evaluated with the F-quasi-likelihood test and the false discovery rate (FDR) was used to correct for multiple testing according to the Benjamini-Hochberg method. The ontological analysis was performed using three packages from R: topGO (version 2.34.0), clusterProfiler (version 3.10.1) and pathview (version 1.22.3). Significant genes were analyzed using the Kyoto Encyclopedia of Genes and Genomes (KEGG) database looking for their impact on functional pathways.

Analysis was performed three times: using all regulated genes, using up-regulated genes, and using down-regulated genes only. The union of these three analyses was performed to provide a single list of results. Gene enrichment analysis was performed with and without including FDRs found in the initial DGE. Analysis for transcription factors was performed using orthologous genes between the mouse and the human with the DAVID Functional Annotation Tool (v6.8). Orthologous genes are aggregated in FAST DB from Ensemblcompara. The same thresholds and methods were used as GO terms and Pathway analysis but with human data.

The mRNA expression of lipocalin 2 (*Lcn2*), a known MR target, was verified by RT-qPCR and normalized to the *Rpl8* housekeeping gene using the following rat primers: *Lcn2*: forward, 5'-TCA CCC TGT ACG GAA GAA CC-3', reverse, 5'-GGT GGG AAC AGA GAA AAC GA-3'; Rpl8: forward, 5'-TGC TAA CCG AGC TGT TGT TG-3', reverse 5'-CTC CAC AGG ATT CAT GGC AA-3'.

2.4. Nephrectomy/aldosterone/salt (NAS) model in mice

For chronic exposure of the RPE-choroid complex to aldosterone, we created the NAS model in mice which is commonly used to study the complications of mineralocorticoid and salt overload in the heart, the vessels and the kidney (Sakamuri et al., 2016). Three months old male wild-type C57BL/6 mice were used. Mice were uni-nephrectomized and osmotic minipumps (Charles River Laboratory, L'Arbresle, France) delivering aldosterone (200 µg/kg/day; Sigma-Aldrich, St-Quentin-Fallavier, France) were implanted subcutaneously. The day after surgery, the drinking water was supplemented with 1% NaCl. Mice were maintained on normal chow. In sham-treated animals, the kidney was exposed but not removed. Six weeks later, mice were killed by cervical dislocation.

Systolic blood pressure (SBP) was measured by tail-cuff plethysmography in trained conscious mice using a BP2000 Visitech model. SBP was measured every day in the same

room at the same hour for 5 consecutive days during the last week of NAS treatment. The SBP measurements presented are the average of the last 3 days.

2.5. Posterior segment morphology

Enucleated eyes were fixed in 2.5% glutaraldehyde in cacodylate buffer (0.1 M, pH 7.4). After 30 min, eyes were dissected at the level of the limbus and lenses were removed. The posterior part was fixed for a further 5 hours, dehydrated in a graded alcohol series (50%, 70%, 95% and 100%) and embedded in epoxy resin. Semithin sections (1µm) were cut and stained with toluidine blue. Ultrathin sections (80 nm) were contrasted by uranyl acetate and lead citrate and observed with a transmission electron microscope and photographed.

2.6. Quantitative PCR

RPE-choroid complexes were carefully dissected from enucleated eyes, snap-frozen in liquid nitrogen and stored at -80°C until use. Total RNA was isolated from tissues using the RNeasy Mini Kit including DNase I treatment. First-strand complementary DNA was synthesized from the total mRNA using random primers (ThermoFisher Scientific, Saint Aubin, France) and SuperScript II reverse transcriptase (ThermoFisher Scientific). Transcript levels of genes listed in Table 1 were analyzed by quantitative PCR performed in CFX384 Touch Real-Time PCR Detection System with SYBR Green detection. *Hprt1*, *Ubc* and *18S* were used as housekeeping genes. Delta CT threshold calculation was used for relative quantification of results.

2.7. Immunohistochemistry

Enucleated eyes were fixed in 4% PFA for 2 hours, then snap frozen in Tissue-Tek OCT compound (Bayer Diagnostics, Puteaux, France). Cryosections (10 µm) were collected on slides. After permeabilization with 0.1% Triton X100 and saturation with 5% goat serum, sections were incubated with rabbit anti-nitrotyrosine antibody (NT, 1:100, Bioss, CliniScience, Nante, France) or rabbit anti-4 hydroxynonenal antibody (4HNE,1:100, Abcam, Cambridge, UK) for 1 hour. After washing, Alexa Fluor 488-conjugated goat anti-rabbit IgG (1:200, Thermo Fisher Scientific) were applied for 1 hour. Cell nuclei were stained with 4',6-Diamidino-2-Phenyl-Indole (DAPI, 1:5000, Sigma-Aldrich). Negative controls were performed without primary antibodies. Images were taken using a fluorescence microscope (Olympus BX51, Rungis, France).

2.8. Statistics

Quantitative data were expressed as mean ± SE. Statistical analysis was made using the Graphpad Prism 5 program (Graphpad Software, San Diego, CA, USA). Mann-Whitney test was used to compare two groups. $P < 0.05$ was considered significant.

3. Results

3.1. High dose aldosterone induced posterior segment inflammation in rat

Before IVT, the retinal fundus (Figure 1A and E) and OCT (Figure 1B and F) showed normal vascular network and stratified retinal structure in all rats. We observed signs of intraocular inflammation in 5 out of 6 rats (10 out of 12 eyes) injected with 100 nM aldosterone. Bright-field fundus images showed dilated and tortuous retinal veins (Figure 1G, black arrow heads) compared to intact fundus of sham-injected rats (Figure 1C). On OCT, we observed an increase in retinal thickness (Figure 1H, double-headed arrow), choroidal vascular dilation (closed arrows) and infiltration of inflammatory cells in the vitreous (between open arrows in H) in aldosterone-injected eyes. Posterior synechia was also observed in 5 eyes out of 12 injected with aldosterone impeding fundus examination. In none of the eyes (n=12) injected with saline, signs of inflammation were observed demonstrating that the inflammatory reaction was due to the high dose of aldosterone injected into the vitreous.

3.2. Transcriptomic regulation in the rat RPE-choroid complex at 24 hours after aldosterone intravitreous injection

We excluded from the transcriptomic analysis the only rat from the aldosterone group that did not show any signs of inflammation in the posterior segment and we pooled RNA from both eyes of each of other rats. The RNAseq analysis was thus performed on 5 aldosterone samples and 6 sham samples that showed two distinct transcriptomic profiles, although the aldosterone samples had a more heterogeneous distribution than the sham group (Figure 2A). When comparing the two groups, there were 2803 significantly differentially regulated genes, 1712 were up-regulated and 1091 were down regulated (Figure 2B). Figure 3 shows colorimetric representation of the most significant up- and down-regulated GO-terms. Most of the up-regulated genes code for proteins of the inflammatory response, neutrophil chemotaxis, response to IL1, IL6 and IL12, TNF and genes coding for proteins involved in RNA processing, which is expected since aldosterone is a transcription factor. Synaptic activity and neurotransmitters appear to be the more significantly down-regulated by aldosterone. Figure 4 and 5 show gene concept networks with colorimetric representation of the fold change in

expression of individual up-regulated genes, classified by GO-terms without FDR filter (Figure 4) and with FDR filter (Figure 5). Up-regulated genes encoding interleukins and chemokines or their receptors are encircled in red and the matrix metallopeptidases (MMP) genes are in blue. According to the clinical phenotype, inflammatory genes are up-regulated such as interleukin 1, 6, 17 and 23 and *Sdf1/Cxcr4*. Other inflammatory genes coding proteins involved in the NF-kB and TNF-alpha pathways, CCL3, CXCL1, CCL2/CCR2 axis were up-regulated. *Lcn2*, highlighted in black in Figure 4 was up-regulated as confirmed by quantitative PCR (Supplementary Figure 1). The gene expression of *Mmp3*, *Mmp9* and *Mmp8* were up-regulated also potentially contributing to the outer retinal barrier breakdown and to retinal edema. Figure 5 shows the individual up-regulated genes encoding proteins in angiogenesis, oxidative stress and MAP kinase cascade. Genes encoding various pro or anti-angiogenic are up-regulated after acute aldosterone injection such as *Fgf2* or *Il1b* (pro) and *Thbs1* and *Angptl4* (anti), but interestingly none of the VEGF family pathway genes are regulated in the RPE-choroid. Figure 6 and 7show gene concept networks with colorimetric representation of the fold change in expression of individual down-regulated genes, classified by GO-terms without FDR filter (Figure 6) and with FDR filter (Figure 7). Numerous genes encode transporters of the solute carrier (SLC) family and the ABCC subfamily (encircled in green), and the bestrophin-2 (*Best2*) anion channel. Other genes, directly linked to the function and the structure of the epithelial barrier were down-regulated, particularly *Shroom2, Cldn1, Cldn2, Cldn22*, *Cdh18*, *Pcdh10* and *Pcdh17*, *Patj* and *Cdc141* (encircled in purple). Numerous genes encoding collagen isoforms (in blue) were also down-regulated suggesting remodeling of the extracellular matrix. Interestingly, *Nr3c2*, which encodes MR was down-regulated as well as *Atp1a2* and *Atp1b1* and *Sgk1* suggesting a negative regulatory loop resulting from high and acute dose on aldosterone in the vitreous. Of note, the Na^+/K^+ ATPase alpha 2 is known to be expressed in RPE cells and it is a known target of aldosterone (Clausen et al., 2017). Genes involved in smooth muscle contraction were down-regulated (*Mylk, Calm2, Acta2, Myh11, Calm1, Lmod1 and Actg2*) which could contribute to the observed vasodilation of choroid vessels. Finally, genes involved in circadian entrainment and in melanogenesis (*Wnt11, Fzd3, Fzd4, Fzd5, Fzd6, Plcb4, Prkcb, Tcf7l2, Prkaca, Camk2a, Gnao1, Calm1 and Calm2*) were deregulated by aldosterone. Table 2 shows the KEGG pathways regulated by aldosterone. Figures 8 to 12 show examples of detailed KEGG pathways, with a colorimetric representation of the fold change (FC) for up- and down-regulated genes within each of the KEGG pathways. KEGG pathway analysis showed a significantly increased expression of the inflammatory cytokines and chemokines implicated

in the Cytokine-cytokine receptor interaction pathway, such as *Ccl3, Ccl3l1, Cxcl1, Cxcl2, Cxcl3, Csf3, Il1, Il6, Il17* and *Il23*. Some of these chemokines are also up-regulated in the TNF signaling pathway where an up-regulation of the receptor *Tnfr2* is also noticed. The up-regulation of *Il1β* stimulates the NF-κB signaling pathway and the production of MIP-2. IL-17 signaling pathway induces the production of AP-1, G-CSF, and different matrix metalloproteinases, chemokines and inflammatory cytokines. Interestingly, genes in the cardiac muscle contraction KEGG pathway are down-regulated which could contribute to the vasodilation.

In summary, aldosterone induces in the RPE-choroid complex, the expression of genes involved in the inflammatory response, particularly neutrophil chemotaxis, regulation of transcription, oxidative stress, extracellular remodeling, synapsis and muscle contraction, cellular metabolism and transports, cytoskeleton and cell junctions, and necroptosis.

3.3. Phenotype of the NAS model

As expected in this mouse model the blood pressure moderately increased by around 15%, the mean SBP in NAS mice was 137.3 ± 6.10 mmHg (mean ± SE) compared to 116.7 ± 2.82 mmHg (mean ± SE) in control mice. The difference was statistically significant (unpaired t-test, p=0.0153, n=5 in each group).

3.4. Morphological alterations in the retina of NAS mice

Compared to intact retinal structure in control mice (Figure 13A-B), NAS mice showed retinal edema in the outer nuclear layer and in the photoreceptor segments (Figure 13C, D and E, white arrows). Elongation and disorganization of photoreceptor segments suggests disturbance of phagocytosis by RPE cells (Figure 13C). Pigment and RPE migration were also observed focally (Figure 13, black arrows in C and inset). We also found RPE cell swelling (Figure 13C inset) and dilation of choroidal vessels (Figure 13D, double arrow).

Ultrathin sections revealed morphological alterations mostly presented in the RPE and photoreceptor segments in NAS mice. The depolarized RPE cells were swollen and filled with numerous vacuoles (Figure 14C and D, asterisks). Their mitochondria were also dilated (Figure 14D). The microvilli of RPE cells were elongated and lost contact with photoreceptor segments (Figure 14C), while in control mice, RPE microvilli were in close contact with photoreceptor segments (Figure 14B). The outer segments of photoreceptors were disorganized and their size appeared heterogeneous (Figure 14C). In some area, photoreceptor

segments were almost absent and replaced by vacuoles and tissue debris. Pigments and RPE cells migrated into subretinal spaces beyond the RPE level (Figure 14D).

3.5. Gene deregulation in the RPE-Choroid complex of NAS mice

As morphological modifications induced by NAS were presented predominantly in the RPE and photoreceptor segments, we hypothesized dysfunction of RPE cells. We assessed gene regulation of the RPE-choroid complexes in the NAS mouse model (Figure 15). While the expression of MR and GR remained unchanged, mRNA transcripts of HSD2 enzyme were up-regulated in NAS mice. The *Atp1b2*, one of the Na^+/K^+ ATPase subunits, anion pump whose expression is known to be induced by aldosterone, was also increased, suggesting enhanced MR activation. Genes involved in inflammation and fibrosis, such as *Tnfα*, *Cox2*, *Icam1* and *Cxcr4* were deregulated in the RPE-choroid complex of NAS mice. For *Lcn2* and *Lgals3* (encoding Gal-3 protein) genes, despite a tendency to be increased, the difference was not significant compared to control mice. The expression of NOX subunits, involved in ROS synthesis and reflecting oxidative stress, were also dysregulated with an up-regulation of *Nox2* and an elevated ration of *Nox2/Nox4* while the expression of *Nox4* was unchanged. Up-regulation of *Mmp3* could be implicated in the permeability of blood-retinal barrier. *Shroom2* that controls the contractility and morphology of endothelial cells was increased. Gene encoding *Angptl4*, a regulator of angiogenesis that inhibits endothelial migration and proliferation, was decreased in NAS mice. *Per1*, a gene important to the maintenance of circadian rhythms in cells, was also down-regulated in the PRE-choroid complex of NAS mice.

Overall, genes involved in inflammatory response, oxidative stress, cell contractility and migration and angiogenesis were deregulated in the RPE-choroid complex of NAS mice and several of these genes were in common with genes regulated in the acute aldosterone injection model.

3.6. Increase in oxidative stress in the retina and RPE-Choroid complex of NAS mice

To assess the stress events in the retina of NAS mice, we performed immunostaining of nitrotyrosine (NT) and 4HNE on retinal sections, which are markers of nitrosative stress and lipid peroxidation respectively. While a faint NT staining could be detected in the ganglion cell layer (GCL), the inner nuclear layer (INL) and the inner segment (IS) of photoreceptors of control mice (Figure 16A and B), more intense and diffuse NT immunostaining was

detected in the retinal layers of the NAS mice retinas (Figure 16C and D). In addition, NT accumulate in the RPE cells of NAS mice (Figure 16C, inset) indicating a nitrosative stress. The retina of control mice showed a diffused immunostaining of 4HNE (Figure 16E and F), whereas in NAS mice, 4HNE labeling was enhanced in the outer nuclear layer (Figure 16G and H), suggesting an increase in lipid peroxidation in the photoreceptors.

4. Discussion

Acute intraocular injection of aldosterone (100nM) in the Lewis rat eye induced vasodilation of choroidal vessels, increased retinal thickness, retinal vessel dilation and tortuosity and cell infiltration in the vitreous at 24 hours. This acute effect was observed in 10 out of 12 aldosterone-injected eyes and in none of the 12 sham-injected eyes, suggesting that the acute inflammation was due to aldosterone itself. Lipocalin 2 (LCN2), a known biomarker of MR activation in the cardiovascular system (Latouche et al., 2012) was increased in the RPE-choroid complex of eyes injected with aldosterone, except in the two eyes from the same animal that did not develop an inflammatory reaction (supplementary Figure 1), justifying that we did exclude this outlier rat from the RNA-Seq transcriptome analysis. Interestingly, the *Lcn2* expression increase in response to aldosterone varied between animals, suggesting endogenous differential susceptibility to aldosterone. In previous studies we showed that while lower acute vitreous aldosterone dose (20nM) induced retinal edema (Zhao et al., 2010) and choroidal vessel dilation (Zhao et al., 2012) it did not induce cellular infiltration. It is unlikely that such a high aldosterone concentration could ever reach the eye vitreous, even in case of primary aldosteronism, in which lower systemic levels were measured (Baron et al., 2018). In addition, we could not detect any aldosterone in the ocular media of the normal rat eye, using either mass spectrometry methods (Travers et al., 2017) or radio-immunoassay (personal unpublished data), suggesting that aldosterone transport to the eye must be highly regulated, protecting the retina from aldosterone exposure.

The reason for testing a high aldosterone dose was to ensure the delivery of at least 10nM aldosterone to the RPE apical side, as no more than 10% of the injected dose of glucocorticoid was found to reach the retina after intravitreous administration (Chang-Lin et al., 2011). Our experiment shows that high dose of aldosterone that is physiologically not present in the vitreous, induces an inflammatory reaction. Interestingly, when the ocular barriers are compromised like in retinal vein occlusion, the systemic and sustained release of low aldosterone dose (0.83 µg/day) aggravated retinal edema and monocytes infiltration in the

retina, suggesting that aldosterone could exert different effects depending nit only on the dose but also on the inflammatory state of the retina (Allingham et al., 2018).

The proinflammatory effect of aldosterone and/or MR pathway activation is known in the heart, the blood vessels and in the kidney (Brown, 2013). It has also been demonstrated in the brain, where aldosterone infused systemically (at 2µg/100g/day in rats), synergized with lipopolysaccharide to induce the brain expression of IL-1β and IL-6, concomitant to depressive behavior (Bay-Richter et al., 2012). At the dose used in our experiment, aldosterone activates the MR but possibly also the GR (Mani et al., 2016) in ocular cells, which effect on inflammation still remain to be understood (De Bosscher et al., 2016).

At 24 hours after the intravitreous injection of 100 nM aldosterone, *Nr3c2* that encodes MR and *Sgk1* genes were down-regulated suggesting a negative feedback loop. The decreased expression of *Nr3c2* could also have contributed to the inflammatory reaction, as it was shown to occur in ocular tissues as early as 3 hours after LPS injection (Bousquet et al., 2012). The transcriptomic regulation in the RPE-choroid complex at 24 hours confirmed the activation of genes involved in the inflammatory response, such as, *Il1β*, *Il6*, *Il17*, *Lcn2* and genes involved in the NF-κB, TNF-α and neutrophil chemotaxis pathways. Chemokines gene expression, such as *Ccr2*, *Ccl2* and *Cxcr4* were up-regulated. IL-17 signaling pathway is known to be induced by aldosterone in other organs (Herrada et al., 2010) and CXCR4 to be increased by MR pathway activation in T cells (Besedovsky et al., 2014). Interestingly, the SDF-1/CXCR4 pathway has been shown to intervene in the angiogenic process in the laser-induced choroidal neovascularization model (Sengupta et al., 2010) and to be regulated in the RPE and choroid of human macula at different stages of age-related macular degeneration (AMD), with more intense expression in the RPE and choroid in early AMD eyes (Bhutto et al., 2006). This is in line with the observation that MR antagonists reduced choroidal neovascularization in the rodent laser-induced model in a VEGF-independent manner (Zhao et al., 2019). Interestingly, upon activation of CXCR4, RPE cells were shown to migrate (Crane et al., 2000), suggesting a role in the breakdown of the RPE barrier. Neutrophil infiltration has also been involved in RPE barrier breakdown through MMP proteins expression (Zhou et al., 2010) and particularly the NGAL/MMP9 axis has been shown to intervene in RPE-choroid complex pathology and in AMD in human eyes (Ghosh et al., 2017). NGAL (LCN in rodent) is a known marker of MR activation in the heart, the vessels and in the kidney (Gilet et al., 2015; Gorini et al., 2018; Latouche et al., 2012). The up-regulation of *Lcn2* gene in the RPE-choroid complex, following acute aldosterone intravitreal

injection, correlated with the inflammatory response induced by aldosterone. Numerous genes encoding proteins that form or regulate intercellular junctions, such as claudins, cadherins and cytoskeleton regulators were down-regulated by aldosterone, contributing to the weakening of the outer retinal barrier.

The expression of genes encoding transporters were down-regulated by acute aldosterone such as oxysterol binding protein-like 6 (*Osbpl6*), that regulates the transcellular transport of cholesterol and the Na^+/K^+ ATPase subunit alpha 2 (*Atp1a2*). The Na^+/K^+-ATPase subunit alpha 2 serves as an ion pump creating an electrochemical gradient across the plasma membrane, that is essential for transepithelial transport, cell volume regulation and osmotic control in polarized epithelium such as RPE cells, but also for the electrical activity of nerve and muscle cells (Clausen et al., 2017) that regulate the vascular tone in the choroid. Other genes, involved in smooth muscle contraction were down-regulated (*Mylk, Calm2, Acta2, Myh11, Calm1, Lmod1* and *Actg2*) potentially contributing to the choroidal vasodilation observed after aldosterone injection. Interestingly, mutations in *Mylk,* encoding the myosin light chain kinase, *Acta2* and *Myh11* genes have been associated with vascular aneurysms (Takeda and Komuro, 2019). In pachychoroid, the focal enlargement of choroidal vessels could also potentially correspond to aneurysmal dilation. Numerous genes involved in axon guidance and the neuromuscular junction were also regulated by aldosterone, which could contribute as well to the abnormal vascular tone of choroidal vessels submitted to acute aldosterone injection. Another interesting finding is the regulation of genes involved in synaptic transmission. This could be expected as choroidal nerves from the sympathetic and parasympathetic systems are very dense in the choroid as they control the choroidal vascular flow (Reiner et al., 2018). Particularly, Nerve fibers containing vasoactive intestinal polypeptide (VIP) exert vasodilatory action on choroidal blood vessels (Jablonski et al., 2007) and pachychoroid has been associated with allelic variants of *vipr2* gene (Hosoda et al., 2018). The effect of aldosterone on the choroid could also be related to the regulation of genes involved in the function of the choroidal nerves. Altogether, it appears that aldosterone administered acutely via the intraocular route and eventually reaching the apical side of the RPE and the choroid, is pathogenic and regulates numerous RPE and choroidal genes. This observation shows that MR pathway activation by aldosterone delivered through the apical side of the RPE is pathogenic for the RPE-choroid complex. In addition, this model could be used to further study the pro-inflammatory mechanisms of aldosterone in ocular tissues. One limitation of this study is that we have analyzed the RPE/ choroid complex without separation of the RPE from the choroid, which does not allow to get the specific gene regulation induced

by aldosterone in each cell types or in each specific layer. Other techniques, using microdissection or single cell RNA seq are required to perform a more targeted analysis. Another manuscript reporting the effect of aldosterone on RPE cells from human iPS cells is currently under preparation, with the limitation of a more artificial experimental setting.

To better explore the role of aldosterone in a more physiological context, we used the NAS mouse model, commonly used to study the cardiovascular and kidney complications of aldosterone /MR pathway activation (Clausen et al., 2017). In this model, aldosterone is constantly infused leading to a high aldosterone exposure of the choroid and the baso-lateral side of the RPE. In this model, systemic aldosterone is increased like in condition in which the renin-angiotensin-aldosterone is activated. But, the hypertension in this model is moderate (about 15% of systolic blood pressure increase), excluding that the ocular phenotype could result from hypertension alone. Choroidal vasodilation and retinal edema were common features of the acute aldosterone injection model in rat and, the NAS model in mice. However, in the NAS model, no cell infiltration was observed, although fluid accumulation was clearly present in the outer retina and the RPE barrier was disrupted by migration of RPE cells in the sub retinal space, as confirmed by TEM. Interestingly, an elongation of photoreceptor outer segments with accumulation of non-digested segments was present focally, suggesting a dysfunction of the RPE cells. We did not observe sub-retinal fluid accumulation in this mouse model, although non-cellular sub-retinal deposit could be found. The phenotype of NAS mice shows alteration of the RPE-choroid complex but no obvious alteration of the inner retina. The *Atp1b2* gene, encoding the Na^+/K^+ ATPase transporting subunit beta 2 (Clausen et al., 2017), was up-regulated in the RPE-choroid complex. While MR and GR expression was not modified in NAS mice, the expression of HSD2, an enzyme that prevents illicit activation of MR by glucocorticoids, was up-regulated, suggesting that circulating aldosterone could have accessed MR in the RPE-choroid complex and directly activated the receptor. Similar regulations were found in the acute aldosterone and the NAS model, such as for the TNF-alpha pathway and the *Cxcr4* and *Mmp3* genes. On the other hand, several genes were regulated in both models but in the opposite direction, such as *Angplt4* and *Per1*, which can be explained by the different kinetic of the aldosterone stimulation. Nevertheless, in both models, gene involved in the inflammatory response, oxidative stress, cell migration and RPE metabolism were regulated. More specifically, the NOX pathway was activated in the RPE/ choroid from NAS mice, with an increase in *nox2* expression, leading to the production of superoxide that can react in the cells with NO to produce the reactive molecule peroxynitrite, which causes the nitrosylation of proteins

(Brandes et al., 2014). In the retina from NAS mice, nitrotyrosine could be identified in different cell layers and more specifically in the RPE. Moreover, lipid peroxidation, identified by 4-HNE staining was also observed in the retina from NAS mice. Interestingly, Nox2 is also activated by AngII in vascular endothelial cells (Daiber et al., 2017) and in the retina (Wilkinson-Berka et al., 2013) and, prorenin activates NOX in RPE cells (Haque et al., 2017) showing that different molecules of the RAAS activate common oxidative stress pathways. As expected, defense mechanisms are activated as observed in the transcriptome from RPE/ choroid submitted to acute aldosterone (Fig 5), in which several genes, encoding anti-oxydant proteins are upregulated such as *sod1* and *sod2*. These superoxide dismutase enzymes transform superoxide into hydrogen peroxide and diatomic oxygen .*sod1* and *sod2* (Azadmanesh and Borgstahl, 2018). COX2 induced in the RPE by outer segment phagocytosis, that seemed defective in the NAS mouse eye, and involved in choroidal vasculature (Houssier et al., 2008), was up-regulated in RPE-choroid complex from NAS mice.

None of the two aldosterone exposure models described herein, recapitulates all features of a human retinal disease. Nevertheless, the NAS mouse model shows interesting features of pachychoroid pigment epitheliopathy (Cheung et al., 2018), including choroidal vessel dilation, RPE pigment loss, RPE cells migration in the retina and a pro-angiogenic environment. In addition, genes regulated by acute activation of the MR pathway in the RPE-choroid complex by aldosterone injection, encodes proteins involved in the RPE barrier disruption through cell migration, alteration of the extra cellular matrix and in cellular junctions, in smooth muscle and neurovascular control, and regulation of ion transport and cell volume, that could contribute to the pathogenesis of pachychoroid associated diseases, including CSCR.

In conclusion, these two different models of ocular aldosterone exposure share some common phenotypic and molecular features at the RPE-choroid complex level. However, the inflammation status differs significantly, whether aldosterone is administrated in the vitreous or via the systemic circulation and whether the aldosterone stress is acute or chronic, emphasizing the complexity of corticosteroid regulations in the retina. These observations also suggest that regulation of MR pathway via the intraocular route or via the systemic route might be different, prompting to develop local MRA formulations. Additional models specifically designed to over or under express corticosteroid receptors in retinal cells could help understand the complex effects of MR/GR pathways activation in retinal physiopathology.

5. Acknowledgements

This work was supported by grants from INSERM, the AgenceNationale de la Recherche (ANR Mineraloret ANR-11-BSV1–0022, ROCK-SUR-MeR ANR-15-CE18–0032 et ANR-16-CE14-0021-01), the Fondation pour la RechercheMédicale (FRM Visual System 2013, DVS20131228894), the EU COST Action BM1301 European Cooperation in Science and Technology ADMIRE-Aldosterone and Mineralocorticoid Receptor Physiology and Pathophysiology (ADMIRE http://www.admirecosteu.com) and the Swiss National Science Foundation (Grant #320030_156401). BB is supported by a PhD ARDoC grant from Region Ile de France. We thank the Centre d'Explorations Fonctionnelles of the Center de Recherche des Cordeliers for their technical support.

6. References

Allingham, M.J., Tserentsoodol, N., Saloupis, P., Mettu, P.S., and Cousins, S.W. (2018). Aldosterone Exposure Causes Increased Retinal Edema and Severe Retinopathy Following Laser-Induced Retinal Vein Occlusion in Mice. Invest. Ophthalmol. Vis. Sci. *59*, 3355–3365.

Azadmanesh, J., and Borgstahl, G.E.O. (2018). A Review of the Catalytic Mechanism of Human Manganese Superoxide Dismutase. Antioxid. Basel Switz. *7*.

Baron, S., Amar, L., Faucon, A.-L., Blanchard, A., Baffalie, L., Faucard, C., Travers, S., Pagny, J.-Y., Azizi, M., and Houillier, P. (2018). Criteria for diagnosing primary aldosteronism on the basis of liquid chromatography-tandem mass spectrometry determinations of plasma aldosterone concentration. J. Hypertens. *36*, 1592–1601.

Bay-Richter, C., Hallberg, L., Ventorp, F., Janelidze, S., and Brundin, L. (2012). Aldosterone synergizes with peripheral inflammation to induce brain IL-1β expression and depressive-like effects. Cytokine *60*, 749–754.

Besedovsky, L., Linz, B., Born, J., and Lange, T. (2014). Mineralocorticoid receptor signaling reduces numbers of circulating human naïve T cells and increases their CD62L, CCR7, and CXCR4 expression. Eur. J. Immunol. *44*, 1759–1769.

Bhutto, I.A., McLeod, D.S., Merges, C., Hasegawa, T., and Lutty, G.A. (2006). Localisation of SDF-1 and its receptor CXCR4 in retina and choroid of aged human eyes and in eyes with age related macular degeneration. Br. J. Ophthalmol. *90*, 906–910.

Biwer, L.A., Wallingford, M.C., and Jaffe, I.Z. (2019). Vascular Mineralocorticoid Receptor: Evolutionary Mediator of Wound Healing Turned Harmful by Our Modern Lifestyle. Am. J. Hypertens. *32*, 123–134.

Bousquet, E., Zhao, M., Ly, A., Leroux Les Jardins, G., Goldenberg, B., Naud, M.-C., Jonet, L., Besson-Lescure, B., Jaisser, F., Farman, N., et al. (2012). The aldosterone-mineralocorticoid receptor pathway exerts anti-inflammatory effects in endotoxin-induced uveitis. PloS One *7*, e49036.

Brandes, R.P., Weissmann, N., and Schröder, K. (2014). Nox family NADPH oxidases: Molecular mechanisms of activation. Free Radic. Biol. Med. *76*, 208–226.

Brooke, S.M., de Haas-Johnson, A.M., Kaplan, J.R., and Sapolsky, R.M. (1994). Characterization of mineralocorticoid and glucocorticoid receptors in primate brain. Brain Res. *637*, 303–307.

Brown, N.J. (2013). Contribution of aldosterone to cardiovascular and renal inflammation and fibrosis. Nat. Rev. Nephrol. *9*, 459–469.

Chang-Lin, J.-E., Attar, M., Acheampong, A.A., Robinson, M.R., Whitcup, S.M., Kuppermann, B.D., and Welty, D. (2011). Pharmacokinetics and pharmacodynamics of a sustained-release dexamethasone intravitreal implant. Invest. Ophthalmol. Vis. Sci. *52*, 80–86.

Cheung, C.M.G., Lee, W.K., Koizumi, H., Dansingani, K., Lai, T.Y.Y., and Freund, K.B. (2018). Pachychoroid disease. Eye Lond. Engl.

Chrissobolis, S. (2017). Vascular Consequences of Aldosterone Excess and Mineralocorticoid Receptor Antagonism. Curr. Hypertens. Rev.

Clausen, M.V., Hilbers, F., and Poulsen, H. (2017). The Structure and Function of the Na,K-ATPase Isoforms in Health and Disease. Front. Physiol. *8*.

Crane, I.J., Wallace, C.A., McKillop-Smith, S., and Forrester, J.V. (2000). CXCR4 receptor expression on human retinal pigment epithelial cells from the blood-retina barrier leads to chemokine secretion and migration in response to stromal cell-derived factor 1 alpha. J. Immunol. Baltim. Md 1950 *165*, 4372–4378.

Daiber, A., Di Lisa, F., Oelze, M., Kröller-Schön, S., Steven, S., Schulz, E., and Münzel, T. (2017). Crosstalk of mitochondria with NADPH oxidase via reactive oxygen and nitrogen species signalling and its role for vascular function. Br. J. Pharmacol. *174*, 1670–1689.

De Bosscher, K., Beck, I.M., Ratman, D., Berghe, W.V., and Libert, C. (2016). Activation of the Glucocorticoid Receptor in Acute Inflammation: the SEDIGRAM Concept. Trends Pharmacol. Sci. *37*, 4–16.
De Kloet, E.R., Vreugdenhil, E., Oitzl, M.S., and Joëls, M. (1998). Brain corticosteroid receptor balance in health and disease. Endocr. Rev. *19*, 269–301.
van Dijk, E.H.C., Nijhoff, M.F., de Jong, E.K., Meijer, O.C., de Vries, A.P.J., and Boon, C.J.F. (2016). Central serous chorioretinopathy in primary hyperaldosteronism. Graefes Arch. Clin. Exp. Ophthalmol. Albrecht Von Graefes Arch. Klin. Exp. Ophthalmol. *254*, 2033–2042.
van Dijk, E.H.C., Schellevis, R.L., van Bergen, M.G.J.M., Breukink, M.B., Altay, L., Scholz, P., Fauser, S., Meijer, O.C., Hoyng, C.B., den Hollander, A.I., et al. (2017). Association of a Haplotype in the NR3C2 Gene, Encoding the Mineralocorticoid Receptor, With Chronic Central Serous Chorioretinopathy. JAMA Ophthalmol. *135*, 446–451.
Ghosh, S., Shang, P., Yazdankhah, M., Bhutto, I., Hose, S., Montezuma, S.R., Luo, T., Chattopadhyay, S., Qian, J., Lutty, G.A., et al. (2017). Activating the AKT2-nuclear factor-κB-lipocalin-2 axis elicits an inflammatory response in age-related macular degeneration. J. Pathol. *241*, 583–588.
Gilet, A., Zou, F., Boumenir, M., Frippiat, J.-P., Thornton, S.N., Lacolley, P., and Ropars, A. (2015). Aldosterone up-regulates MMP-9 and MMP-9/NGAL expression in human neutrophils through p38, ERK1/2 and PI3K pathways. Exp. Cell Res. *331*, 152–163.
Golestaneh, N., Picaud, S., and Mirshahi, M. (2002). The mineralocorticoid receptor in rodent retina: ontogeny and molecular identity. Mol. Vis. *8*, 221–225.
Gorini, S., Marzolla, V., Mammi, C., Armani, A., and Caprio, M. (2018). Mineralocorticoid Receptor and Aldosterone-Related Biomarkers of End-Organ Damage in Cardiometabolic Disease. Biomolecules *8*.
Haque, R., Iuvone, P.M., He, L., Hur, E.H., Chung Choi, K.S., Park, D., Farrell, A.N., Ngo, A., Gokhale, S., Aseem, M., et al. (2017). Prorenin receptor (PRR)-mediated NADPH oxidase (Nox) signaling regulates VEGF synthesis under hyperglycemic condition in ARPE-19 cells. J. Recept. Signal Transduct. Res. *37*, 560–568.
Herrada, A.A., Contreras, F.J., Marini, N.P., Amador, C.A., González, P.A., Cortés, C.M., Riedel, C.A., Carvajal, C.A., Figueroa, F., Michea, L.F., et al. (2010). Aldosterone promotes autoimmune damage by enhancing Th17-mediated immunity. J. Immunol. Baltim. Md 1950 *184*, 191–202.
Hindle, S.J., Munji, R.N., Dolghih, E., Gaskins, G., Orng, S., Ishimoto, H., Soung, A., DeSalvo, M., Kitamoto, T., Keiser, M.J., et al. (2017). Evolutionarily Conserved Roles for Blood-Brain Barrier Xenobiotic Transporters in Endogenous Steroid Partitioning and Behavior. Cell Rep. *21*, 1304–1316.
Hosoda, Y., Yoshikawa, M., Miyake, M., Tabara, Y., Ahn, J., Woo, S.J., Honda, S., Sakurada, Y., Shiragami, C., Nakanishi, H., et al. (2018). CFH and VIPR2 as susceptibility loci in choroidal thickness and pachychoroid disease central serous chorioretinopathy. Proc. Natl. Acad. Sci. U. S. A. *115*, 6261–6266.
Houssier, M., Raoul, W., Lavalette, S., Keller, N., Guillonneau, X., Baragatti, B., Jonet, L., Jeanny, J.-C., Behar-Cohen, F., Coceani, F., et al. (2008). CD36 deficiency leads to choroidal involution via COX2 down-regulation in rodents. PLoS Med. *5*, e39.
Jablonski, M.M., Iannaccone, A., Reynolds, D.H., Gallaher, P., Allen, S., Wang, X., and Reiner, A. (2007). Age-related decline in VIP-positive parasympathetic nerve fibers in the human submacular choroid. Invest. Ophthalmol. Vis. Sci. *48*, 479–485.
Kolkhof, P., and Bärfacker, L. (2017). 30 YEARS OF THE MINERALOCORTICOID RECEPTOR: Mineralocorticoid receptor antagonists: 60 years of research and development. J. Endocrinol. *234*, T125–T140.
Lan, N.C., Graham, B., Bartter, F.C., and Baxter, J.D. (1982). Binding of steroids to

mineralocorticoid receptors: implications for in vivo occupancy by glucocorticoids. J. Clin. Endocrinol. Metab. *54*, 332–342.
Latouche, C., El Moghrabi, S., Messaoudi, S., Nguyen Dinh Cat, A., Hernandez-Diaz, I., Alvarez de la Rosa, D., Perret, C., López Andrés, N., Rossignol, P., Zannad, F., et al. (2012). Neutrophil gelatinase-associated lipocalin is a novel mineralocorticoid target in the cardiovascular system. Hypertens. Dallas Tex 1979 *59*, 966–972.
Lim-Tio, S.S., Keightley, M.C., and Fuller, P.J. (1997). Determinants of specificity of transactivation by the mineralocorticoid or glucocorticoid receptor. Endocrinology *138*, 2537–2543.
Lumbers, E.R. (1999). Angiotensin and aldosterone. Regul. Pept. *80*, 91–100.
Mani, O., Nashev, L.G., Livelo, C., Baker, M.E., and Odermatt, A. (2016). Role of Pro-637 and Gln-642 in human glucocorticoid receptors and Ser-843 and Leu-848 in mineralocorticoid receptors in their differential responses to cortisol and aldosterone. J. Steroid Biochem. Mol. Biol. *159*, 31–40.
Matulich, D.T., Spindler, B.J., Schambelan, M., and Baxter, J.D. (1976). Mineralocorticoid receptors in human kidney. J. Clin. Endocrinol. Metab. *43*, 1170–1174.
Nicholson, B.P., Atchison, E., Idris, A.A., and Bakri, S.J. (2018). Central serous chorioretinopathy and glucocorticoids: an update on evidence for association. Surv. Ophthalmol. *63*, 1–8.
Peters, J. (2012). Local renin-angiotensin systems in the adrenal gland. Peptides *34*, 427–432.
Reiner, A., Fitzgerald, M.E.C., Del Mar, N., and Li, C. (2018). Neural control of choroidal blood flow. Prog. Retin. Eye Res. *64*, 96–130.
Sakamuri, S.S.V.P., Valente, A.J., Siddesha, J.M., Delafontaine, P., Siebenlist, U., Gardner, J.D., and Chandrasekar, B. (2016). TRAF3IP2 Mediates Aldosterone/Salt-Induced Cardiac Hypertrophy and Fibrosis. Mol. Cell. Endocrinol. *429*, 84.
Sengupta, N., Afzal, A., Caballero, S., Chang, K.-H., Shaw, L.C., Pang, J.-J., Bond, V.C., Bhutto, I., Baba, T., Lutty, G.A., et al. (2010). Paracrine modulation of CXCR4 by IGF-1 and VEGF: implications for choroidal neovascularization. Invest. Ophthalmol. Vis. Sci. *51*, 2697–2704.
Takeda, N., and Komuro, I. (2019). Genetic basis of hereditary thoracic aortic aneurysms and dissections. J. Cardiol.
Travers, S., Martinerie, L., Bouvattier, C., Boileau, P., Lombès, M., and Pussard, E. (2017). Multiplexed steroid profiling of gluco- and mineralocorticoids pathways using a liquid chromatography tandem mass spectrometry method. J. Steroid Biochem. Mol. Biol. *165*, 202–211.
Wilkinson-Berka, J.L., Tan, G., Jaworski, K., and Miller, A.G. (2009). Identification of a retinal aldosterone system and the protective effects of mineralocorticoid receptor antagonism on retinal vascular pathology. Circ. Res. *104*, 124–133.
Wilkinson-Berka, J.L., Rana, I., Armani, R., and Agrotis, A. (2013). Reactive oxygen species, Nox and angiotensin II in angiogenesis: implications for retinopathy. Clin. Sci. Lond. Engl. 1979 *124*, 597–615.
Zhao, M., Valamanesh, F., Celerier, I., Savoldelli, M., Jonet, L., Jeanny, J.-C., Jaisser, F., Farman, N., and Behar-Cohen, F. (2010). The neuroretina is a novel mineralocorticoid target: aldosterone up-regulates ion and water channels in Müller glial cells. FASEB J. Off. Publ. Fed. Am. Soc. Exp. Biol. *24*, 3405–3415.
Zhao, M., Célérier, I., Bousquet, E., Jeanny, J.-C., Jonet, L., Savoldelli, M., Offret, O., Curan, A., Farman, N., Jaisser, F., et al. (2012). Mineralocorticoid receptor is involved in rat and human ocular chorioretinopathy. J. Clin. Invest. *122*, 2672–2679.
Zhao, M., Mantel, I., Gelize, E., Li, X., Xie, X., Arboleda, A., Seminel, M., Levy-Boukris, R., Dernigoghossian, M., Prunotto, A., et al. (2019). Mineralocorticoid receptor antagonism

limits experimental choroidal neovascularization and structural changes associated with neovascular age-related macular degeneration. Nat. Commun. *10*, 369.
Zhou, J., He, S., Zhang, N., Spee, C., Zhou, P., Ryan, S.J., Kannan, R., and Hinton, D.R. (2010). Neutrophils compromise retinal pigment epithelial barrier integrity. J. Biomed. Biotechnol. *2010*, 289360.

Table 1. Mouse primers for quantitative PCR.

Gene	Sequences	
Hprt1	Forward	5'-TCT AAC TTT AAC TGG AAA GAA TGT C-3'
	Reverse	5'-TCC TTT TCA CCA GCA AGC T-3'
Ubc	Forward	5'-CGG AGT CGC CCG AGG TCA CA-3'
	Reverse	5'-GGG CTC GAC CTC CAG GGT GA-3'
18S	Forward	5'-CGC CGC TAG AGG TGA AAT TC-3'
	Reverse	5'-TCT TGG CAA ATG CTT TCG C-3'
MR	Forward	5'-CCA GAA GAG GGG ACC ACA TA-3'
	Reverse	5'-GGA ATT GTC GTA GCC TGC AT-3'
GR	Forward	5'-TTC GCA GGC CGC TCA GTG TT-3'
	Reverse	5'-TTG GGA GGT GGT CCC GTT GCT-3'
Nox2	Forward	5'-CGC CCT TTG CCT CCA TTC TC-3'
	Reverse	5'-CCT TTC CTG CAT CTG GGT CTC C-3'
Nox4	Forward	5'-GGG CCT AGG ATT GTG TTT AAG C-3'
	Reverse	5'-GGG CGG CTA CAT GCA CAC-3'
Tnf α	Forward	5'-GGG ACA GTG ACC TGG ACT GT-3'
	Reverse	5'-AGT GAA TTC GGA AAG CCC ATT-3'
Icam1	Forward	5'-TCC GCT ACC ATC ACC GTG TAT TC-3'
	Reverse	5'-TGG CCT CGG AGA CAT TAG AGA AC-3'
Cox2	Forward	5'-TTC GGG AGC ACA ACA GAG T-3'
	Reverse	5'-TAA CCG CTC AGG TGT TGC AC-3'
Angptl4	Forward	5'-GGG ACC AAG ACC ATG ACC TC-3'
	Reverse	5'-GTT GCC GTG GGA TAG AGT GG-3'
Per1	Forward	5'-AGG AAF CCT TCC TCA ACC GC-3'
	Reverse	5'-TGG CGG GAA CGC TTT GCT TT-3'
Lgal3	Forward	5'-CAG TGC TCC TGG AGG CTA TC-3'
	Reverse	5'-ATT GAA GCG GGG GTT AAA GT-3'
Lcn2	Forward	5'-ATG TGC AAG TGG CCA CCA CG-3'
	Reverse	5'-CGC ATC CCA GTC AGC CAC AC-3'
Atp1b2	Forward	5'-CCC CAA GTA CCA GGA TCG AC-3'
	Reverse	5'-TCT GAA CAT GCT GAC CCC AG-3'
Hsd2	Forward	5'-ACC CCT GCT TGG CAG CCT ACG GCA-3'
	Reverse	5'-TCA CAT TAG TCA CTG CCT CTG TCT TG-3'
Shroom2	Forward	5'-GGG ATG CTC TGC TCC AAG TG-3'
	Reverse	5'-CGA AGG GGA GCG AGA AGT TT-3'

Mmp3	Forward	5’-CAT CCC CTG ATG TCC TCG TG-3’
	Reverse	5’-AGG GTG CTG ACT GCA TCA AA-3’
Cxcr4	Forward	5’-TCC CGG AAG CAG GGT TCC TTG T-3’
	Reverse	5’-CCC GGA AGC AGG GTT CCT TGT-3’

Table 2. KEGG pathways regulated by aldosterone in the rat RPE-choroid complex.

ID	Description	setSize	enrichmentScore	NES	pvalue	p.adjust
rno05200	Pathways in cancer	113	0.511206488554918	1.7868433068808	0.00106837606837607	0.00860881542699725
rno04060	Cytokine-cytokine receptor interaction	74	0.763224168492714	2.54377401612801	0.00112866817155756	0.00860881542699725
rno05169	Epstein-Barr virus infection	70	0.546585353418317	1.80754394360699	0.00114285714285714	0.00860881542699725
rno05167	Kaposi sarcoma-associated herpesvirus infection	61	0.601940000246987	1.97669113998117	0.00115606936416185	0.00860881542699725
rno05163	Human cytomegalovirus infection	60	0.564979798575138	1.84536744626613	0.00116279069767442	0.00860881542699725
rno04062	Chemokine signaling pathway	52	0.73456709052833	2.34448210626894	0.00117508813160987	0.00860881542699725
rno04380	Osteoclast differentiation	47	0.642587159855868	2.01905433607112	0.001194743130227	0.00860881542699725
rno05152	Tuberculosis	47	0.682397412922957	2.1441409688218	0.001194743130227	0.00860881542699725
rno04621	NOD-like receptor signaling pathway	46	0.694569378133392	2.17693996420948	0.00120048019207683	0.00860881542699725
rno04668	TNF signaling pathway	46	0.779004655301946	2.4415795164905	0.00120048019207683	0.00860881542699725
rno04630	JAK-STAT signaling pathway	41	0.66452510662156	2.05626444614237	0.00120336943441637	0.00860881542699725
rno05202	Transcriptional misregulation in cancer	42	0.659327906727588	2.04613629768528	0.00120772946859903	0.00860881542699725
rno05418	Fluid shear stress and atherosclerosis	42	0.580614779685404	1.80186059707873	0.00120772946859903	0.00860881542699725
rno04145	Phagosome	39	0.582194904551915	1.77527353103155	0.00122249388753056	0.00860881542699725
rno05164	Influenza A	39	0.628922786681353	1.91775978719245	0.00122249388753056	0.00860881542699725
rno04064	NF-kappa B signaling pathway	38	0.646695660187761	1.96362112147757	0.00122850122850123	0.00860881542699725
rno04625	C-type lectin receptor signaling pathway	36	0.663106793550945	1.99324230616581	0.00123609394313968	0.00860881542699725
rno04657	IL-17 signaling pathway	34	0.881197103026261	2.62164919027532	0.00123915737298637	0.00860881542699725
rno05132	Salmonella infection	34	0.794888560687679	2.36487267641853	0.00123915737298637	0.00860881542699725
rno05162	Measles	34	0.65666514798592	1.95364425006287	0.00123915737298637	0.00860881542699725
rno04659	Th17 cell differentiation	37	0.699489530869541	2.10667434626749	0.00124069478908189	0.00860881542699725
rno05140	Leishmaniasis	30	0.712473115886245	2.07422493755065	0.00126262626262626	0.00860881542699725
rno05142	Chagas disease (American trypanosomiasis)	29	0.684278702047603	1.9785276380632	0.00126742712294043	0.00860881542699725
rno04620	Toll-like receptor signaling pathway	31	0.673905145960707	1.95865953370345	0.00127226463104326	0.00860881542699725
rno04640	Hematopoietic cell lineage	26	0.708655462151018	2.00385464998191	0.0012853470437018	0.00860881542699725
rno05133	Pertussis	24	0.746536468894838	2.0678940950985	0.00130039011703511	0.00860881542699725
rno05146	Amoebiasis	23	0.661879754528012	1.81530086808371	0.00130548302872063	0.00860881542699725
rno05321	Inflammatory bowel disease (IBD)	23	0.769733427494049	2.1111051509944	0.00130548302872063	0.00860881542699725
rno05323	Rheumatoid arthritis	19	0.862552065739361	2.27013788207864	0.0013550135501355	0.00860881542699725
rno05144	Malaria	16	0.774149008352663	1.9728321255041	0.00136425648021828	0.00860881542699725
rno05150	Staphylococcus aureus infection	15	0.763827096044658	1.93835134114248	0.00136612021857923	0.00860881542699725
rno05134	Legionellosis	17	0.820835714771193	2.10443568209508	0.00137741046831956	0.00860881542699725
rno04010	MAPK signaling pathway	65	0.522213754213095	1.72715974381469	0.00229095074455899	0.0136323359007566
rno05166	Human T-cell leukemia virus 1 infection	59	0.553857645087639	1.80679937602024	0.00231749710312862	0.0136323359007566
rno04623	Cytosolic DNA-sensing pathway	15	0.723593790017977	1.83625194836204	0.00273224043715847	0.0156128024980484
rno04260	Cardiac muscle contraction	10	-0.696387261608713	-1.97098981651087	0.00303030303030303	0.0163800163800164
rno04740	Olfactory transduction	10	-0.746785788982268	-2.11363312677325	0.00303030303030303	0.0163800163800164
rno04974	Protein digestion and absorption	17	-0.632873848207821	-2.19405495839996	0.0036231884057971	0.01906941266209
rno04610	Complement and coagulation cascades	10	0.779505601492666	1.78206256648821	0.00446428571428571	0.0228937728937729
rno04217	Necroptosis	32	0.583915022063159	1.71350965965207	0.0050125313283208	0.0249836045095406
rno04650	Natural killer cell mediated cytotoxicity	28	0.607569754028458	1.73374050442383	0.00512163892445583	0.0249836045095406
rno04658	Th1 and Th2 cell differentiation	26	0.608073468361933	1.71944042230217	0.006426735218509	0.030603501040519
rno05161	Hepatitis B	39	0.538517360251792	1.64208859985091	0.00855745721271394	0.0398021265707625
rno05168	Herpes simplex virus 1 infection	62	0.486716015979839	1.60068221013618	0.0103806228373702	0.0464171743545112
rno04932	Non-alcoholic fatty liver disease (NAFLD)	23	0.614866806422079	1.6863610645559	0.010443864229765	0.0464171743545112

Legends to Figures

Figure 1. Fundus and optical coherence tomography (OCT) of rat retinas before and 24 hours after intravitreous injection (IVT) of aldosterone.

Fundus (A and E) and OCT images (B and F) before IVT. Fundus (C and G) and OCT images (D and H) 24 hours after sham or aldosterone (Aldo) injection. Aldosterone-injected eyes show dilated and tortuous retinal veins (G, black arrow heads), retinal edema (double-headed arrow in H compared to that in D), choroidal vascular dilation (H, closed arrows) and infiltration of inflammatory cells in the vitreous (between two open arrows).

Green lines indicate the location of OCT scans. Double-headed arrows show the retinal thickness. Closed arrows showed the border of the choroid on OCT. NR, neuroretina; RPE, retinal pigment epithelium; chor, choroid. Bars: 100 µm.

Figure 2. General transcriptomic profiles of aldosterone-injected (Aldo) vs. sham-injected rat RPE-choroid complexes.

A, Multidimensional Scaling (MDS) distribution of rat RPE-choroid samples showing the absence of outliers and of a batch effect. B, Differentially regulated genes between aldosterone (aldo) and sham-injected RPE-choroid samples. Red points indicate significant aldosterone up-regulated genes (1712) and blue points indicate significant aldosterone down-regulated genes (1091).

Figure 3. Colorimetric representation of the most significant up- and down-regulated GO-terms induced by aldosterone in the rat RPE-choroid complex.

Figure 4. Gene concept network for up-regulated genes without FDR induced by aldosterone in the rat RPE-choroid complex.

Genes are represented with a heat colorimetric scale showing the fold change in their expression (red for the highest fold change), and linked to up-regulated GO-terms.

Figure 5. Gene concept network for up-regulated genes with FDR induced by aldosterone in the rat RPE-choroid complex.

Genes are represented with a heat colorimetric scale showing the fold change in their expression (red for the highest fold change), and linked to up-regulated GO-terms.

Figure 6. Gene concept network for down-regulated genes without FDR induced by aldosterone in the rat RPE-choroid complex.
Genes are represented with a heat colorimetric scale showing the fold change in their expression (green for the lowest fold change), and linked to down-regulated GO-terms.

Figure 7. Gene concept network for down-regulated genes with FDR induced by aldosterone in the rat RPE-choroid complex.
Genes are represented with a heat colorimetric scale showing the fold change in their expression (green for the lowest fold change), and linked to down-regulated GO-terms.

Figure 8. Aldosterone-regulated KEGG pathway: Cytokine-cytokine receptor interaction. Log-fold change is shown with a colorimetric scale from green (down-regulation) to red (up-regulation).

Figure 9. Aldosterone-regulated KEGG pathway: TNF signaling pathway (upper) and NF-Kappa B signaling pathway (bottom). Log-fold change is shown with a colorimetric scale from green (down-regulation) to red (up-regulation).

Figure 10. Aldosterone-regulated KEGG pathway: IL-17 signaling pathway. Log-fold change is shown with a colorimetric scale from green (down-regulation) to red (up-regulation).

Figure 11. Aldosterone-regulated KEGG pathway: Cardiac muscle contraction. Log-fold change is shown with a colorimetric scale from green (down-regulation) to red (up-regulation).

Figure 12. Aldosterone-regulated KEGG pathway: Necroptosis. Log-fold change is shown with a colorimetric scale from green (down-regulation) to red (up-regulation).

Figure 13. Semithin retinal sections of NAS mice compared to control mice.
Control mice show intact retinal structure with organized layers (A-B). In NAS mice, fluid accumulates in the outer nuclear layer (ONL) and in the outer segments (OS) of photoreceptors (C, D and E, white arrows). Photoreceptor segments are disorganized and

pigments/retinal pigment epithelial (RPE) cells migrate to the segment layer (C and inset, black arrows). RPE cells and their nuclei are swelling (inset in C). Choroidal vessels are dilated (D, double arrow). INL, inner nuclear layer; IS; inner segments; Chor, choroid. Bars: A, B and E, 50 µm; C, D, F and G, 20 µm.

Figure 14. Retinal ultrastructure of NAS mice compared to control mice.

(A and B) Transmission electron micrographs show that in control mice, retinal pigment epithelium (RPE) locates between photoreceptor segments and the choroid (Chor) with apical membrane microvilli (MV) closely interacting with the outer segments (OS).

(C and D) In NAS mice, OS of photoreceptors are disorganized. In some area, OS are absent. RPE cells are filled with numerous vacuoles (D, asterisks). Mitochondria (M) are round and swelling (D, arrows). Elongated MV of RPE lose close contact with OS. Pigments and dead RPE cells migrate into the subretinal space (D and inset). N, nucleus.

Figure 15. Gene expression in the RPE-choroid complex in NAS mice compared to control mice.

Quantitative PCR data are expressed as mean ± SE. Mann-Whitney test was used. *n*=5 in control (ctrl) and 7 in NAS mice. *Hprt1*, *Ubc*, and *18S* were used as housekeeping genes. *, $p < 0.05$.

Figure 16. Immunoflorescence of Nitrotyrosine and 4HNE in the retina of NAS mice compared to control mice.

(A and B) In control mice, nitrotyrosine (NT) immunofluorescence shows a slight staining in the ganglion cell layer (GCL), the inner nuclear layer (INL) and the inner segment (IS) of photoreceptors. The retinal pigment epithelium (RPE) does not show labeling (arrow and inset). (C and D) In the retina of NAS mice, NT immunostaining is enhanced and appears more diffuse in different retinal layers. RPE cells of NAS mice show NT immunolocalization (arrows and inset).

(E and F) In control mice, 4HNE immunostaining shows diffused points in the retina. (G and H) In NAS mice, 4HNE labeling is enhanced in the outer nuclear layer (ONL).

B, D, F and H are merged images with DAPI. OS, outer segment. Bar: 50 µm.

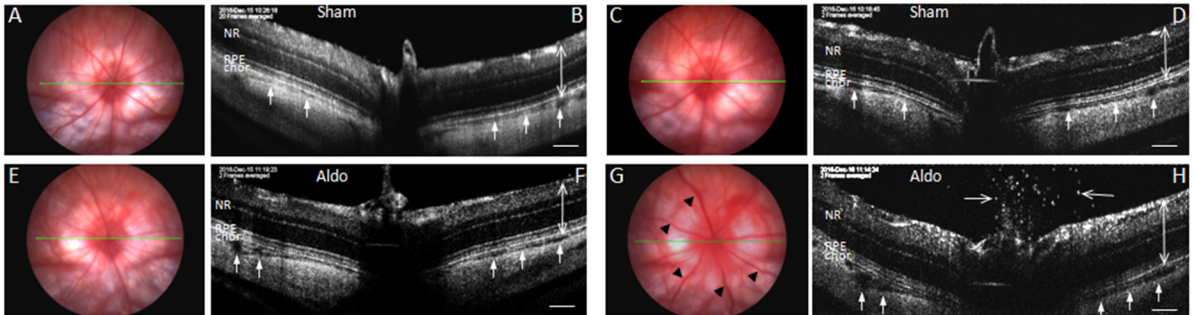
Before IVT
After IVT
A
B
Sham
NR
RPE
Chor
C
D
Sham
NR
RPE
Chor
E
F
Aldo
NR
RPE
Chor
G
H
Aldo
NR
RPE
Chor

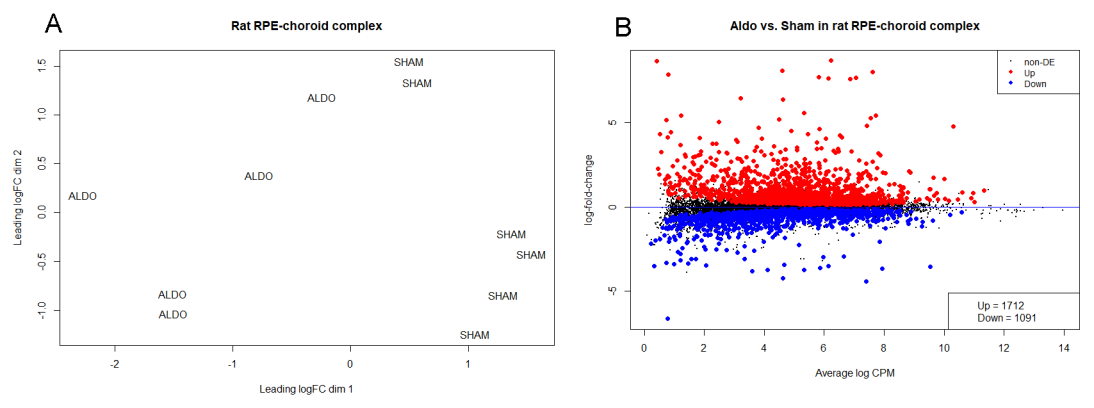
A
Rat RPE-choroid complex
SHAM
SHAM
ALDO
ALDO
ALDO
SHAM
SHAM
ALDO
ALDO
SHAM
Leading logFC dim 2
Leading logFC dim 1
1.5
1.0
0.5
0.0
-0.5
-1.0
-2
-1
0
1
B
Aldo vs. Sham in rat RPE-choroid complex
non-DE
Up
Down
Up = 1712
Down = 1091
log-fold-change
Average log CPM
5
0
-5
0
2
4
6
8
10
12
14

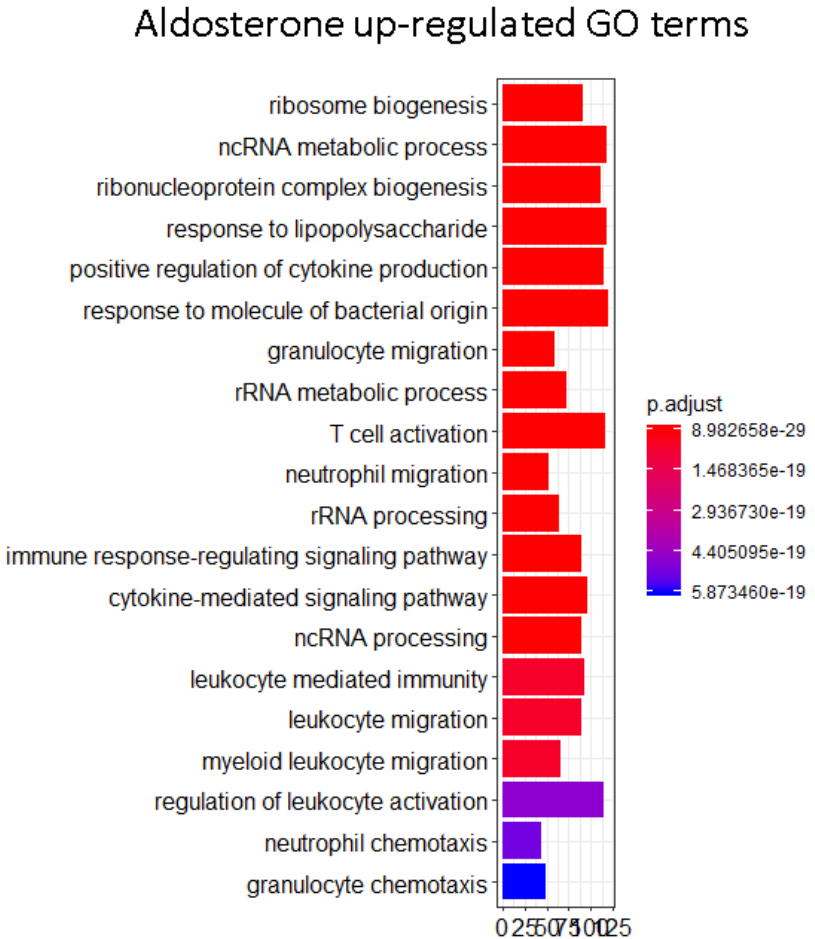
Aldosterone up-regulated GO terms
ribosome biogenesis
ncRNA metabolic process
ribonucleoprotein complex biogenesis
response to lipopolysaccharide
positive regulation of cytokine production
response to molecule of bacterial origin
granulocyte migration
rRNA metabolic process
T cell activation
neutrophil migration
rRNA processing
immune response-regulating signaling pathway
cytokine-mediated signaling pathway
ncRNA processing
leukocyte mediated immunity
leukocyte migration
myeloid leukocyte migration
regulation of leukocyte activation
neutrophil chemotaxis
granulocyte chemotaxis
0 25 50 75 100 125
p.adjust
8.982658e-29
1.468365e-19
2.936730e-19
4.405095e-19
5.873460e-19

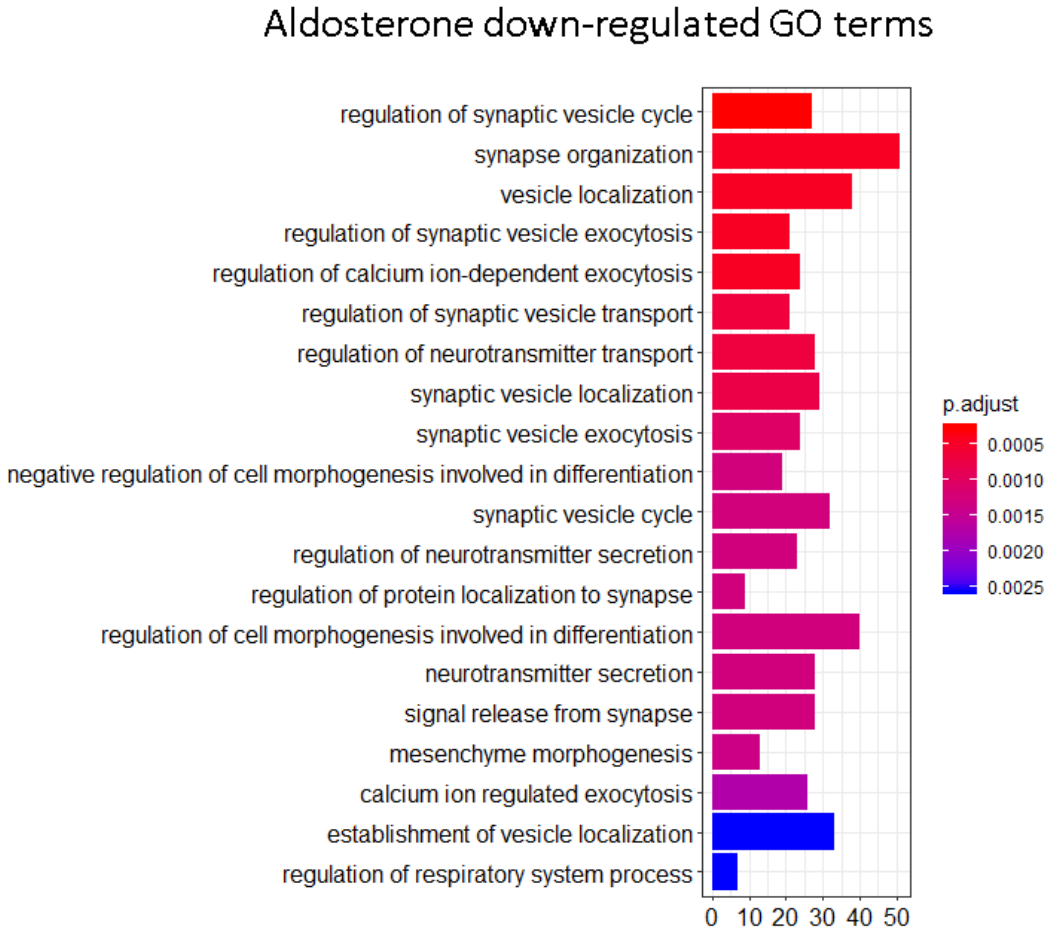
Aldosterone down-regulated GO terms
regulation of synaptic vesicle cycle
synapse organization
vesicle localization
regulation of synaptic vesicle exocytosis
regulation of calcium ion-dependent exocytosis
regulation of synaptic vesicle transport
regulation of neurotransmitter transport
synaptic vesicle localization
synaptic vesicle exocytosis
negative regulation of cell morphogenesis involved in differentiation
synaptic vesicle cycle
regulation of neurotransmitter secretion
regulation of protein localization to synapse
regulation of cell morphogenesis involved in differentiation
neurotransmitter secretion
signal release from synapse
mesenchyme morphogenesis
calcium ion regulated exocytosis
establishment of vesicle localization
regulation of respiratory system process
0 10 20 30 40 50
p.adjust
0.0005
0.0010
0.0015
0.0020
0.0025

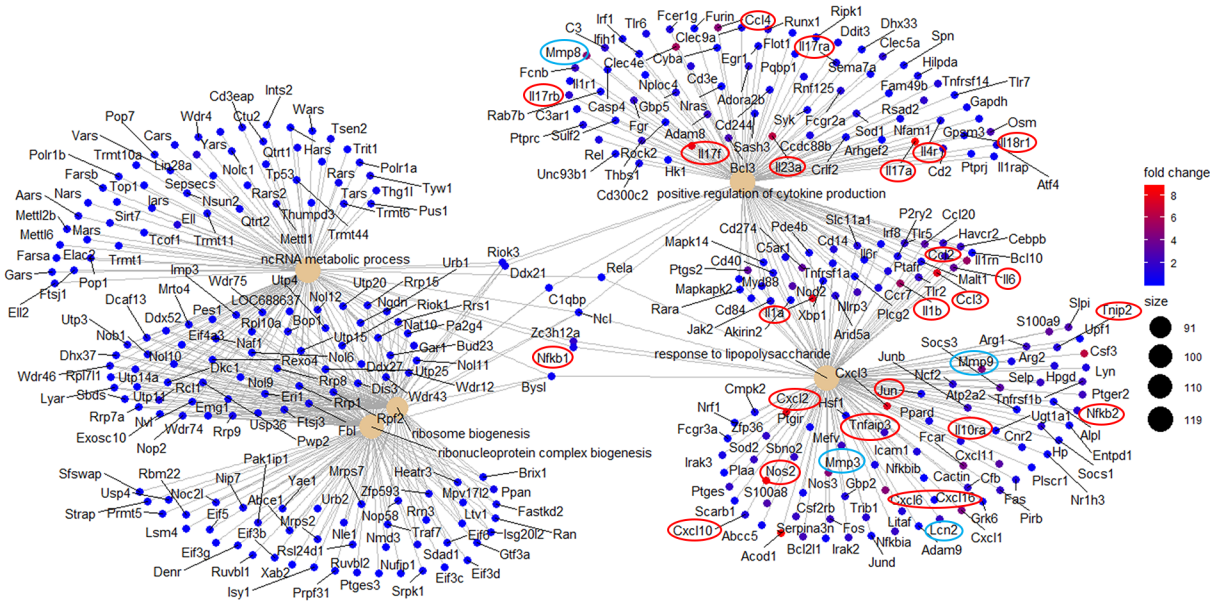
ncRNA metabolic process
positive regulation of cytokine production
response to lipopolysaccharide
ribosome biogenesis
ribonucleoprotein complex biogenesis
fold change
size

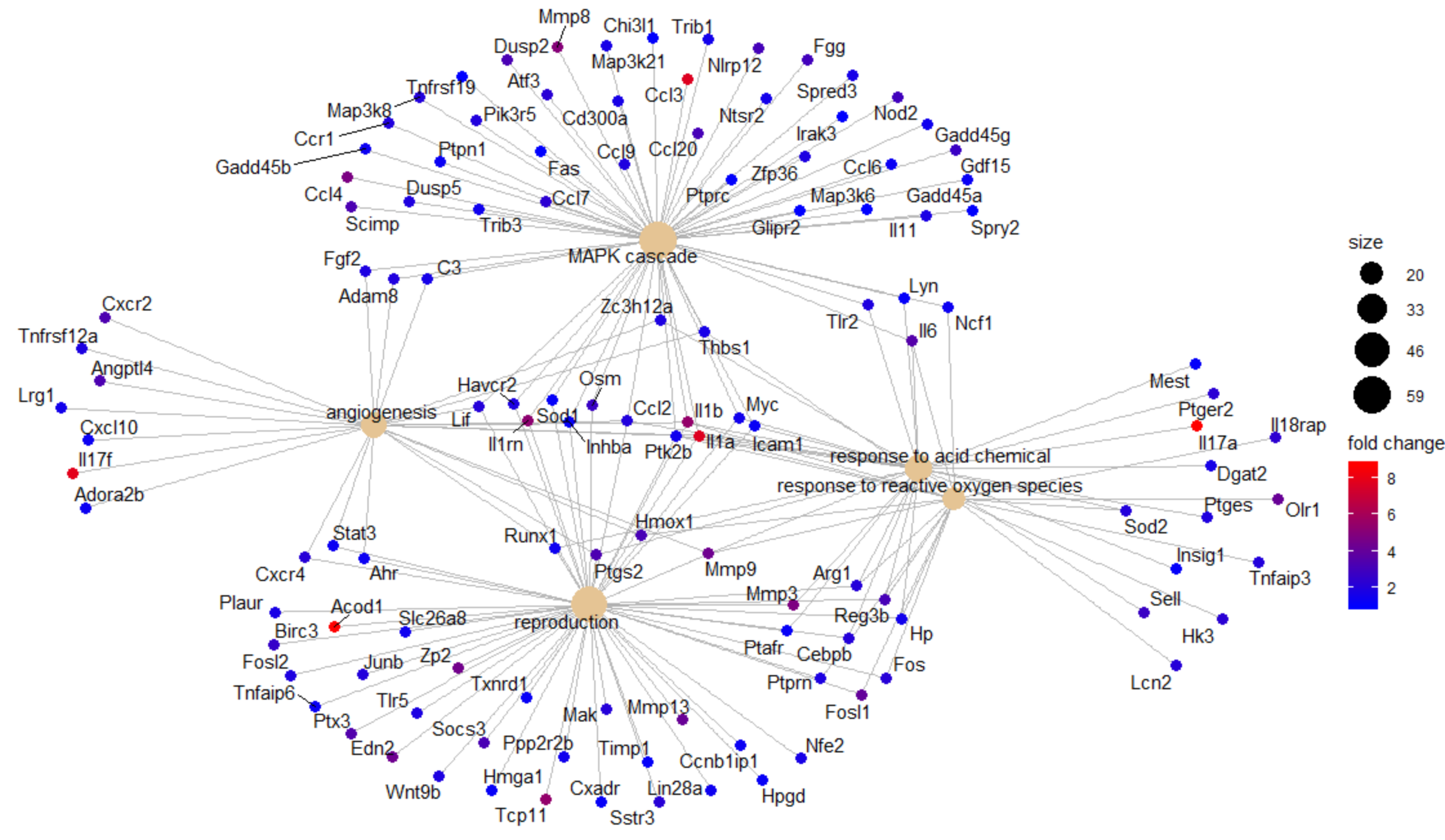
MAPK cascade
angiogenesis
reproduction
response to acid chemical
response to reactive oxygen species
Mmp8
Chi3l1
Trib1
Dusp2
Map3k21
Nlrp12
Fgg
Atf3
Ccl3
Spred3
Tnfrsf19
Map3k8
Pik3r5
Cd300a
Ntsr2
Nod2
Ccr1
Irak3
Gadd45g
Ptpn1
Ccl9
Ccl20
Gadd45b
Fas
Zfp36
Ccl6
Gdf15
Ccl4
Dusp5
Ccl7
Ptprc
Map3k6
Gadd45a
Scimp
Trib3
Glipr2
Il11
Spry2
Fgf2
C3
Adam8
Lyn
Zc3h12a
Tlr2
Ncf1
Il6
Thbs1
Cxcr2
Tnfrsf12a
Angptl4
Lrg1
Cxcl10
Il17f
Adora2b
Havcr2
Osm
Lif
Sod1
Ccl2
Il1b
Myc
Il1rn
Inhba
Ptk2b
Il1a
Icam1
Mest
Ptger2
Il18rap
Il17a
Dgat2
Ptges
Olr1
Sod2
Insig1
Tnfaip3
Sell
Hk3
Lcn2
Stat3
Runx1
Hmox1
Cxcr4
Ahr
Ptgs2
Mmp9
Arg1
Mmp3
Plaur
Acod1
Reg3b
Hp
Slc26a8
Birc3
Ptafr
Cebpb
Fosl2
Junb
Zp2
Fos
Txnrd1
Ptprn
Tnfaip6
Tlr5
Fosl1
Mak
Mmp13
Ptx3
Socs3
Nfe2
Edn2
Ppp2r2b
Timp1
Ccnb1ip1
Hmga1
Cxadr
Lin28a
Hpgd
Wnt9b
Tcp11
Sstr3
size
20
33
46
59
fold change
8
6
4
2

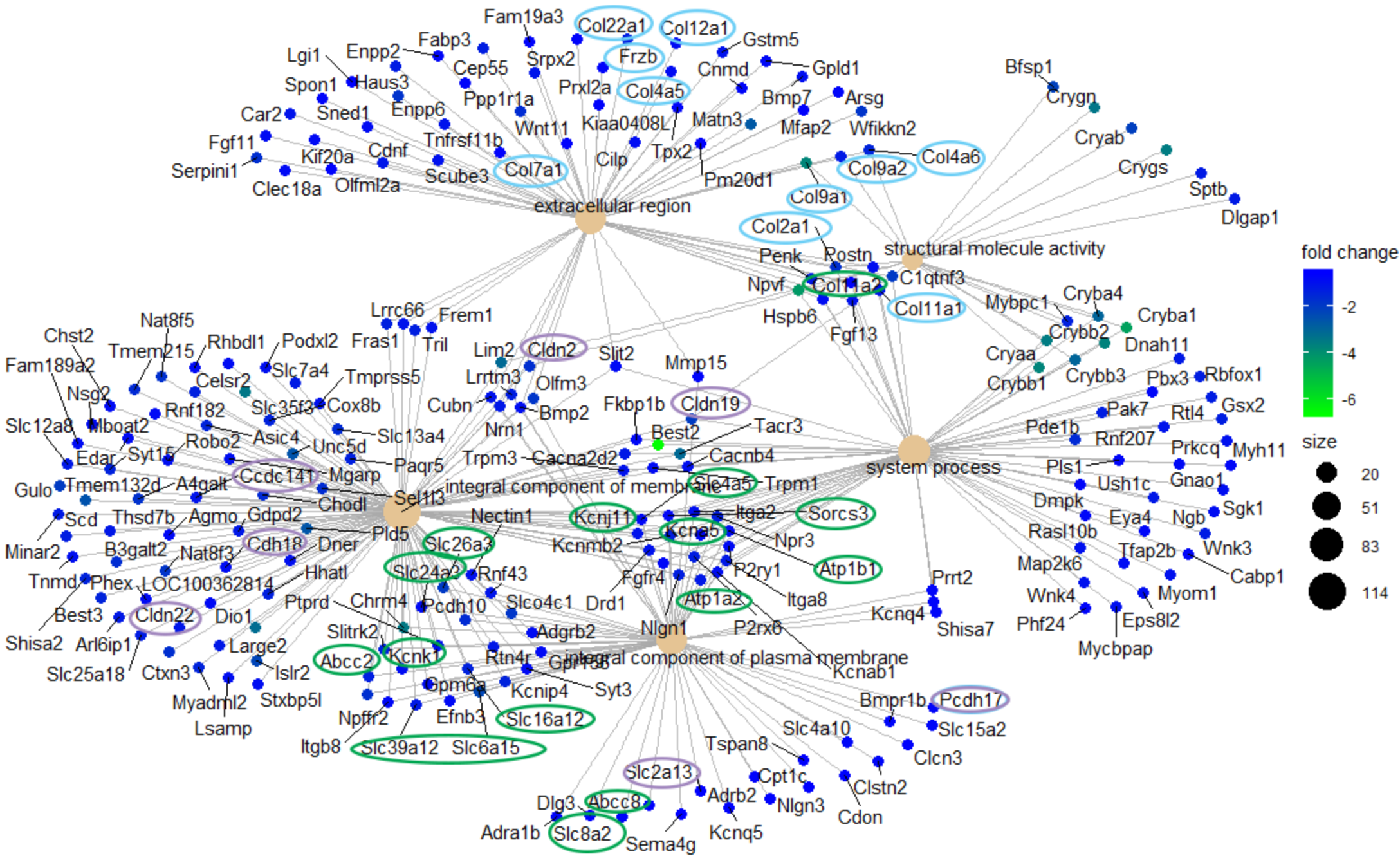
extracellular region
structural molecule activity
system process
integral component of membrane
integral component of plasma membrane
fold change
-2
-4
-6
size
20
51
83
114

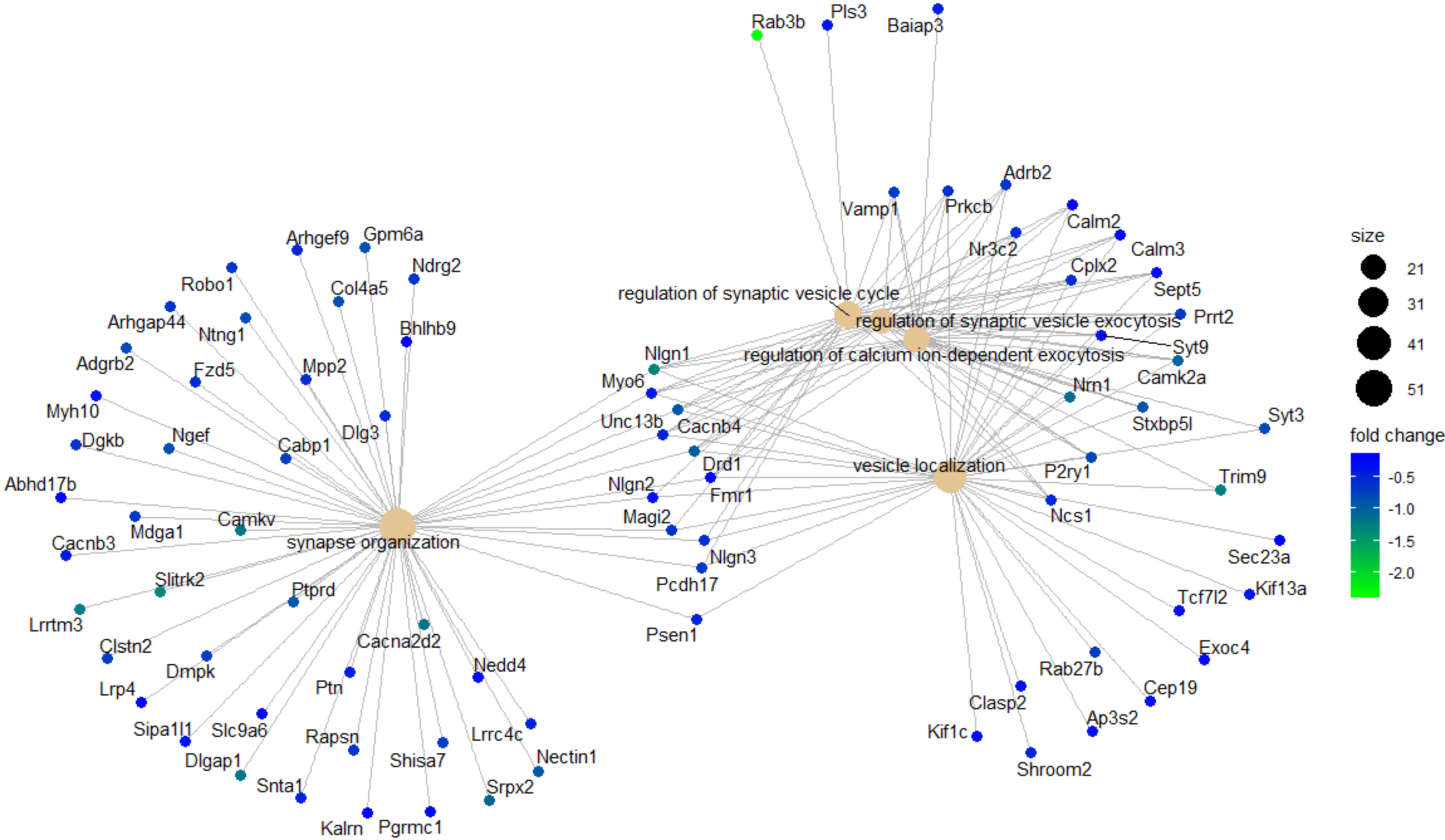
Rab3b
Pls3
Baiap3
Adrb2
Vamp1
Prkcb
Calm2
Nr3c2
Calm3
Cplx2
Sept5
Prrt2
Syt9
Camk2a
Nrn1
Stxbp5l
Syt3
Trim9
P2ry1
Ncs1
Sec23a
Kif13a
Tcf7l2
Exoc4
Rab27b
Cep19
Ap3s2
Clasp2
Kif1c
Shroom2
regulation of synaptic vesicle cycle
regulation of synaptic vesicle exocytosis
regulation of calcium ion-dependent exocytosis
vesicle localization
Nlgn1
Myo6
Unc13b
Cacnb4
Drd1
Nlgn2
Fmr1
Magi2
Nlgn3
Pcdh17
Psen1
Arhgef9
Gpm6a
Ndrg2
Robo1
Col4a5
Arhgap44
Ntng1
Bhlhb9
Adgrb2
Fzd5
Mpp2
Myh10
Dgkb
Ngef
Cabp1
Dlg3
Abhd17b
Mdga1
Camkv
synapse organization
Cacnb3
Slitrk2
Ptprd
Lrrtm3
Clstn2
Cacna2d2
Dmpk
Nedd4
Lrp4
Ptn
Sipa1l1
Slc9a6
Rapsn
Lrrc4c
Dlgap1
Shisa7
Nectin1
Snta1
Srpx2
Kalrn
Pgrmc1
size
21
31
41
51
fold change
-0.5
-1.0
-1.5
-2.0

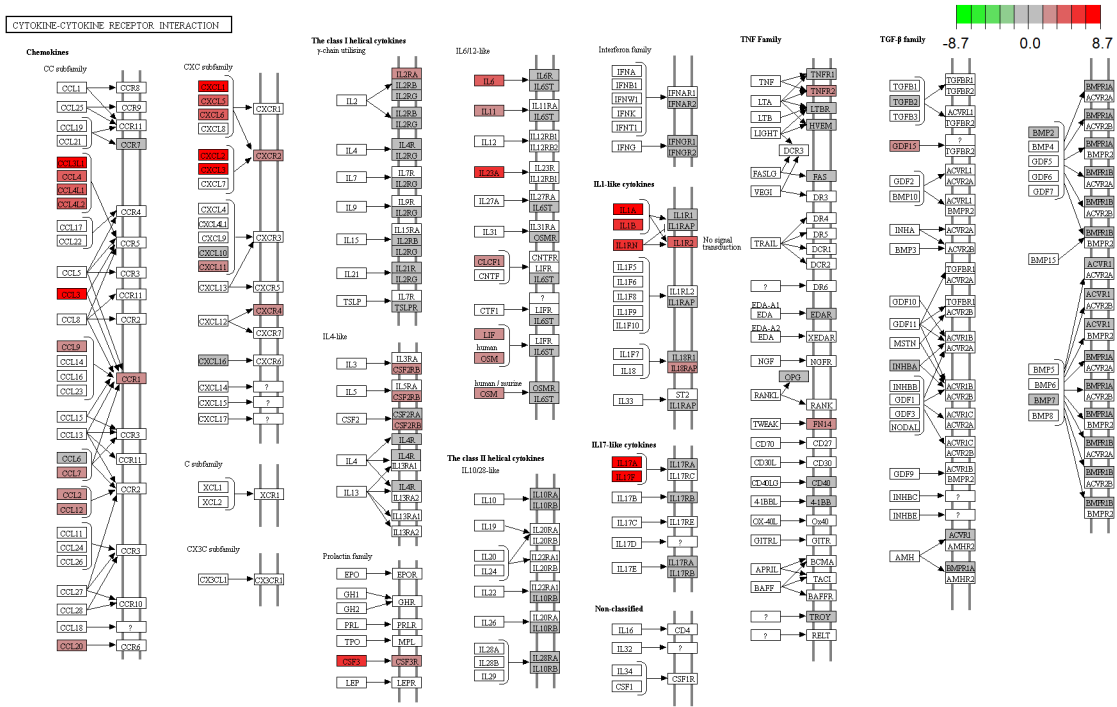
CYTOKINE-CYTOKINE RECEPTOR INTERACTION
-8.7
0.0
8.7
Chemokines
CC subfamily
CXC subfamily
C subfamily
CX3C subfamily
The class I helical cytokines
γ-chain utilizing
IL6/12-like
IL4-like
Prolactin family
The class II helical cytokines
IL10/20-like
Interferon family
IL1-like cytokines
No signal transduction
IL17-like cytokines
Non-classified
TNF Family
TGF-β family
Data on KEGG graph
Rendered by Pathview

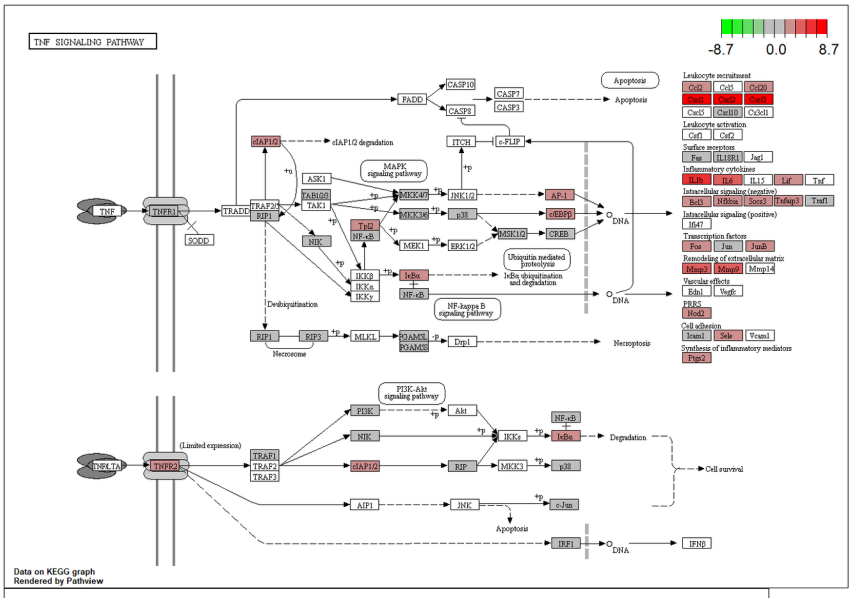
TNF SIGNALING PATHWAY
-8.7
0.0
8.7
TNF
TNFR1
TRADD
TRAF2/5
RIP1
FADD
CASP10
CASP8
CASP7
CASP3
Apoptosis
cIAP1/2
cIAP1/2 degradation
ITCH
c-FLIP
MAPK signaling pathway
ASK1
TAB1/2/3
TAK1
MKK4/7
JNK1/2
AP-1
MKK3/6
p38
C/EBPβ
MSK1/2
CREB
DNA
TpI2
NF-κB
MEK1/2
ERK1/2
Ubiquitin mediated proteolysis
IκBα ubiquitination and degradation
IKKB
IKKα
IKKγ
IκBα
NF-κB
NF-kappa B signaling pathway
Desbiquitination
RIP1
RIP3
MLKL
PGAM5L
PGAM5S
Drp1
Necroptosis
Necrosome
Leukocyte recruitment
Cxl2
Cxl5
Cxl20
Cxl1
Cxl2
Cxl3
Cxl3
Cxl10
Cx3cl1
Leukocyte activation
Csf1
Csf2
Surface receptors
Fas
IL1SR1
Jag1
Inflammatory cytokines
IL1b
IL6
IL12
Lif
Tnf
Intracellular signaling (negative)
Bcl3
IFNBeta
Socs2
TnfAip3
Tnfi
Intracellular signaling (positive)
Ifi47
Transcription factors
Fos
Jun
Junb
Remodeling of extracellular matrix
Mmp3
Mmp9
Mmp14
Vascular effects
Edn1
Vegfc
FRRS
Nos2
Cell adhesion
Icam1
Sele
Vcam1
Synthesis of inflammatory mediators
Ptgs2
TNFLTA
TNFR2
(Limited expression)
PI3K-Akt signaling pathway
PI3K
Akt
NF-κB
IKKε
IκBα
Degradation
TRAF1
TRAF2
TRAF3
NIK
cIAP1/2
RIP
MKK3
p38
Cell survival
AIP1
JNK
c-Jun
Apoptosis
IRF1
DNA
IFNB
Data on KEGG graph
Rendered by Pathview
NF-KAPPA B SIGNALING PATHWAY
-8.7
0.0
8.7
MHC/Antigen
TCR
Lck
Zap
LAT
PLCγ1
Calcium signaling pathway
DAG
IP3
PKCθ
T cell receptor signaling pathway
Antigen
BCR
Syk
Lyn
BLNK
Btk
PLCγ2
PKCβ
B cell receptor signaling pathway
Genotoxic agent
DNA damage
PARP1
PIASy
Ubc9
ATM
NEMO
SUMOylation
Shuttling
NEMO
PIDD
RIP1
Apoptosis
ELKS
IL-1β
IL-1R
MyD88
IRAK1/4
TRAF6
cIAP1/2
Auto-ubiquitination
TNFα
TNF-R1
RIP1
TRADD
TRAF2/5
CYLD
EDA-A1
EDAR
EDARADD
TRAF6
EDA-A2
XEDAR
TRAF3
TRAF6
Virus
RIG-I
TRIM25
TRAF36
LBP
LPS(G-)
CD14
MD-2
TLR4
TIRAP
MyD88
IRAK1/4
TRAF6
TRAM
TRIF
RIP1
TRAF6
Toll-like receptor signaling pathway
Cytokine-cytokine receptor interaction
CD40L
CD40
cIAP1/2
TRAF6
TRAF3
TRAF2
RANKL
RANK
TRAF6
TRAF2
Osteoclast differentiation
LTA
LTB
LIGHT
LTβR
TRAF2
TRAF5
NIK
TRAF2
TRAF3
BAFF
BAFF-R
TRAF2
TRAF3
cIAP1/2
EDA-A2
XEDAR
TRAF3
TRAF6
CARMA
Bcl10
MALT1
Proteasome
Ubiquitin mediated proteolysis
NEMO
IKKα
IKKβ
(S32, S36)
IκBα
Degradation
p50
p65
NFκB
Canonical pathway
TAK1
TAB
Btk
RIG-I-like receptor signaling pathway
Pervanadate, Hypoxia / Reoxygenation (H/R), H2O2, EOF, CNTF, NGF
(Y42)
IκBα
Degradation
p50
p65
NFκB
UV, HER2
CK2
(S/T (PEST))
IκBα
Degradation
p50
p65
NFκB
Atypical pathways
NIK
IKKα
(S866, S870)
Partial degradation
p100
RelB
NFκB
p52
Noncanonical pathway
DNA
cIAP1/2
c-FLIP
XIAP
Bcl-XL
Bcl-2
TRAF1/2
A1/Bfl-1
p100
(Antigen, TNF-α)
Survival
Activation of noncanonical pathway
IL8
IL-1β
TNF-α
A20
IκBα
COX2
(TNF-α, IL-1β, LPS)
Survival
Positive feedback
Negative feedback
Inflammation
MIP-1β
MMP-9
VCAM-1
(TNF-α)
Inflammation
uPA
(H/R)
Bcl-XL
(HGF)
Survival
Bcl-XL
A1/Bfl-1
(UV)
Survival
BLC
ELC
SLC
SDF-1α
BAFF
ICAM
(LT/LIGHT)
Lymphoid-tissue homing
Myelopoiesis and B-cell lymphopoiesis
B-cell development, B-cell survival
Lymphocyte adhesion, T-cell costimulation
Data on KEGG graph
Rendered by Pathview

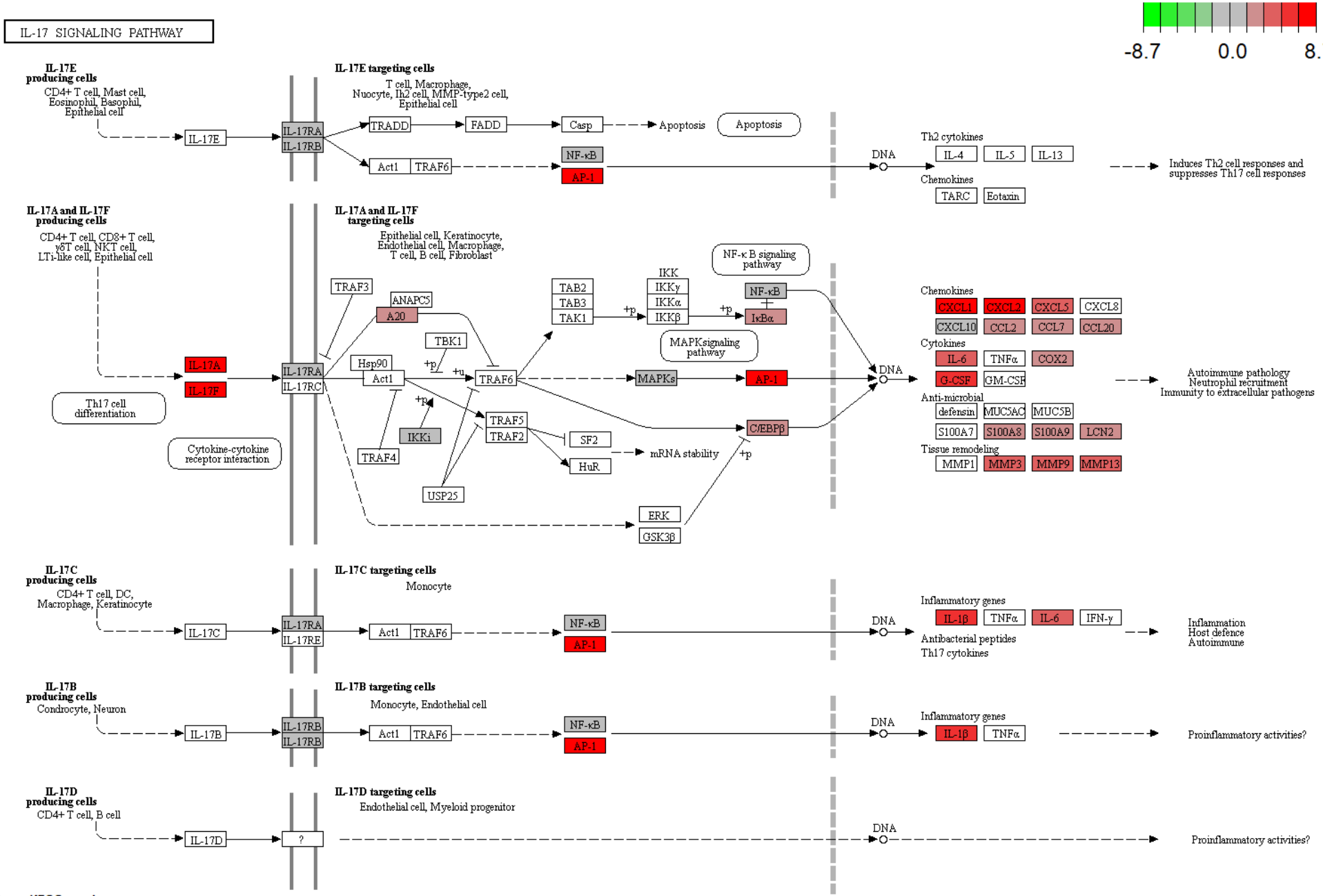
IL-17 SIGNALING PATHWAY
-8.7
0.0
8.7
IL-17E producing cells
CD4+ T cell, Mast cell, Eosinophil, Basophil, Epithelial cell
IL-17E
IL-17E targeting cells
T cell, Macrophage, Nuocyte, Ih2 cell, MMP-type2 cell, Epithelial cell
IL-17RA
IL-17RB
TRADD
FADD
Casp
Apoptosis
Apoptosis
Act1
TRAF6
NF-κB
AP-1
DNA
Th2 cytokines
IL-4
IL-5
IL-13
Chemokines
TARC
Eotaxin
Induces Th2 cell responses and suppresses Th17 cell responses
IL-17A and IL-17F producing cells
CD4+ T cell, CD8+ T cell, γδT cell, NKT cell, LTi-like cell, Epithelial cell
IL-17A
IL-17F
Th17 cell differentiation
Cytokine-cytokine receptor interaction
IL-17A and IL-17F targeting cells
Epithelial cell, Keratinocyte, Endothelial cell, Macrophage, T cell, B cell, Fibroblast
IL-17RA
IL-17RC
TRAF3
ANAPC5
A20
TBK1
Hsp90
Act1
TRAF4
IKKi
USP25
TRAF5
TRAF2
TRAF6
TAB2
TAB3
TAK1
IKK
IKKγ
IKKα
IKKβ
NF-κB signaling pathway
NF-κB
IκBα
MAPKsignaling pathway
MAPKs
AP-1
C/EBPβ
SF2
HuR
mRNA stability
ERK
GSK3β
DNA
Chemokines
CXCL1
CXCL2
CXCL5
CXCL8
CXCL10
CCL2
CCL7
CCL20
Cytokines
IL-6
TNFα
COX2
G-CSF
GM-CSF
Anti-microbial
defensin
MUC5AC
MUC5B
S100A7
S100A8
S100A9
LCN2
Tissue remodeling
MMP1
MMP3
MMP9
MMP13
Autoimmune pathology
Neutrophil recruitment
Immunity to extracellular pathogens
IL-17C producing cells
CD4+ T cell, DC, Macrophage, Keratinocyte
IL-17C
IL-17C targeting cells
Monocyte
IL-17RA
IL-17RE
Act1
TRAF6
NF-κB
AP-1
DNA
Inflammatory genes
IL-1β
TNFα
IL-6
IFN-γ
Antibacterial peptides
Th17 cytokines
Inflammation
Host defence
Autoimmune
IL-17B producing cells
Condrocyte, Neuron
IL-17B
IL-17B targeting cells
Monocyte, Endothelial cell
IL-17RB
IL-17RB
Act1
TRAF6
NF-κB
AP-1
DNA
Inflammatory genes
IL-1β
TNFα
Proinflammatory activities?
IL-17D producing cells
CD4+ T cell, B cell
IL-17D
IL-17D targeting cells
Endothelial cell, Myeloid progenitor
?
DNA
Proinflammatory activities?
Data on KEGG graph
Rendered by Pathview

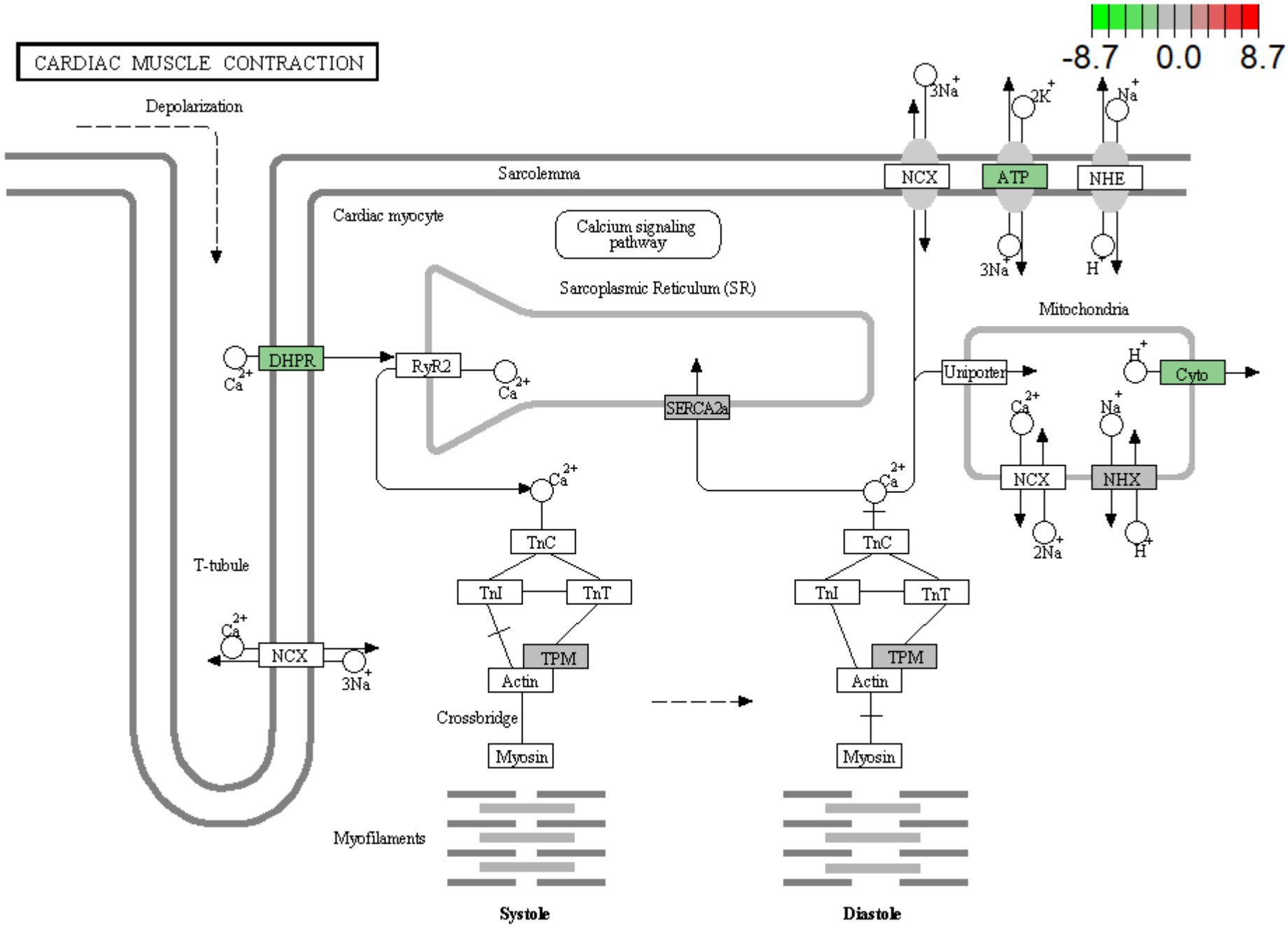
CARDIAC MUSCLE CONTRACTION
-8.7
0.0
8.7
Depolarization
Sarcolemma
Cardiac myocyte
Calcium signaling pathway
Sarcoplasmic Reticulum (SR)
Mitochondria
T-tubule
DHPR
RyR2
SERCA2a
NCX
ATP
NHE
Uniporter
Cyto
NHX
TnC
TnI
TnT
TPM
Actin
Crossbridge
Myosin
Myofilaments
Systole
Diastole
Data on KEGG graph
Rendered by Pathview

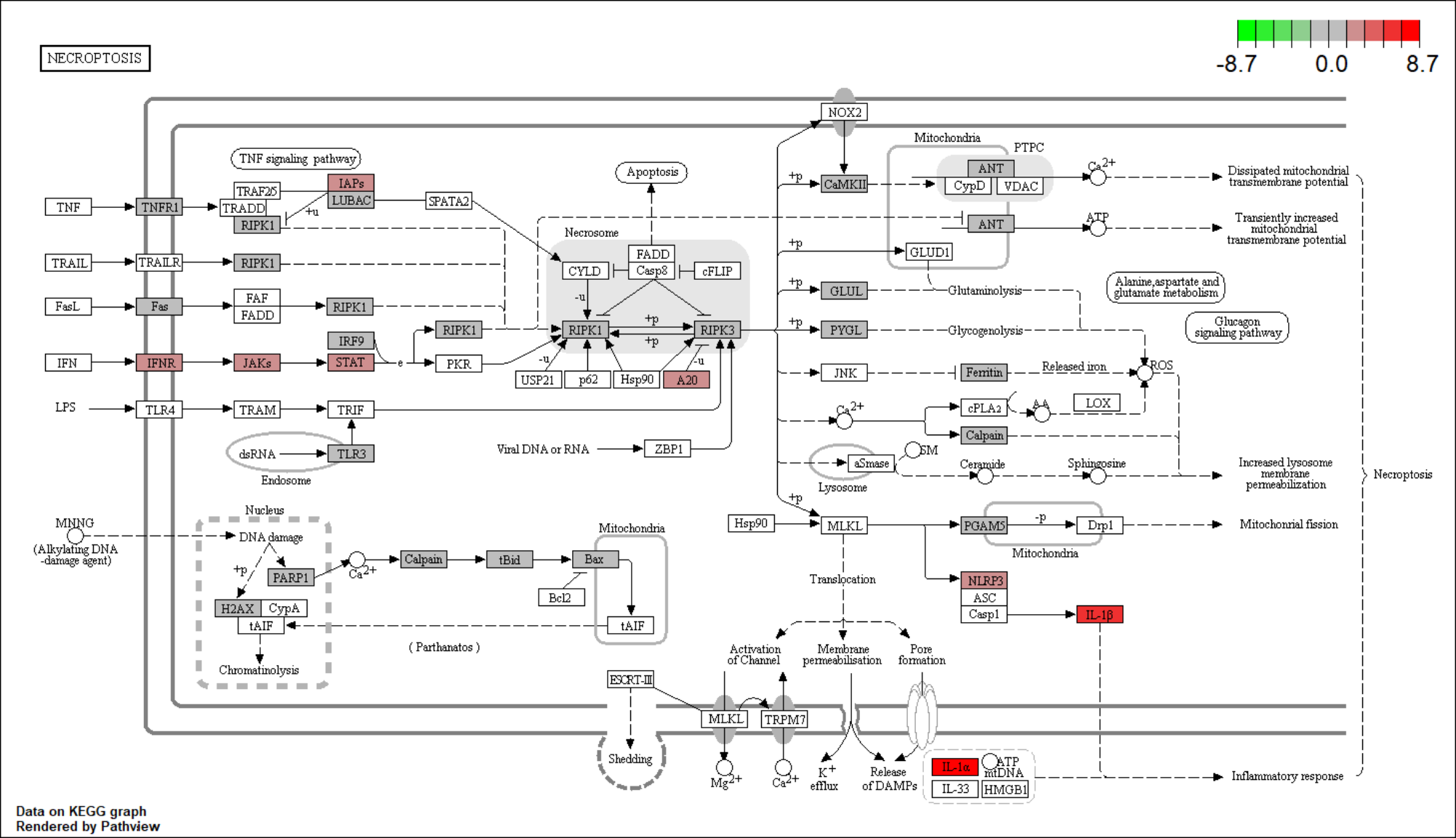

Data on KEGG graph
Rendered by Pathview

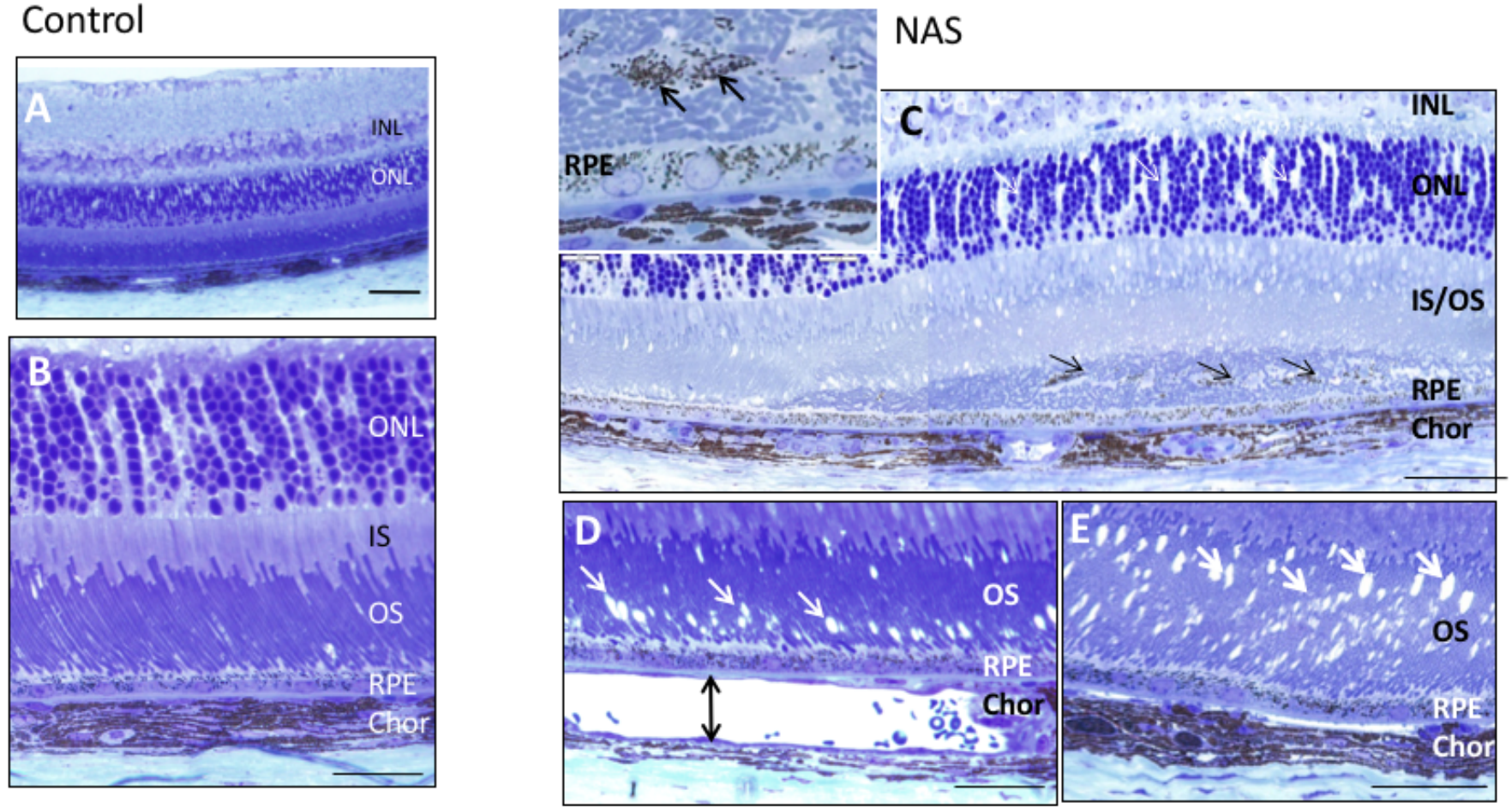
Control
A
INL
ONL
B
ONL
IS
OS
RPE
Chor
NAS
RPE
C
INL
ONL
IS/OS
RPE
Chor
D
OS
RPE
Chor
E
OS
RPE
Chor

Control

NAS

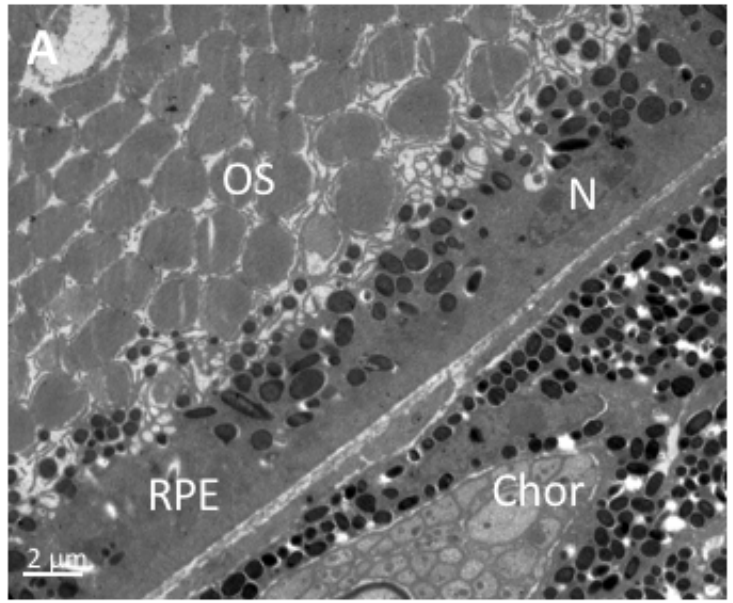
A
OS
N
RPE
Chor
2 µm

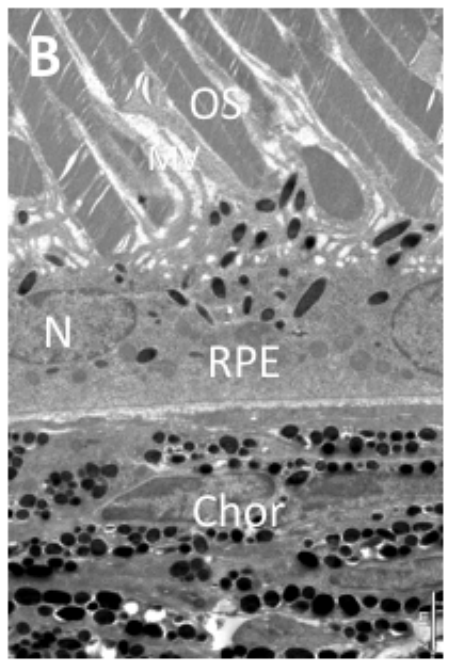
B
OS
MV
N
RPE
Chor

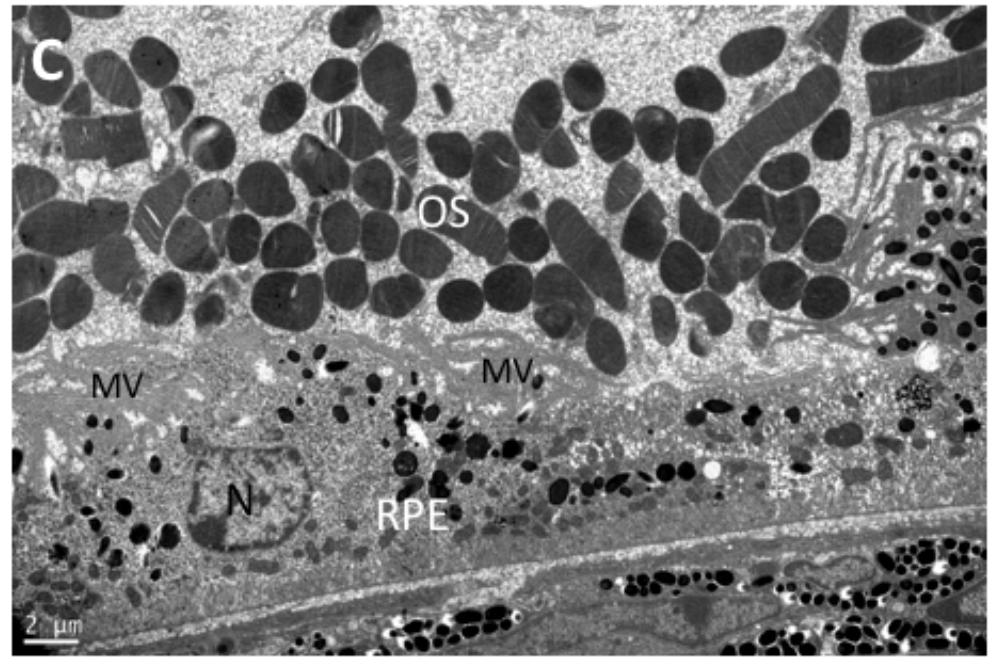
C
OS
MV
MV
N
RPE
2 µm

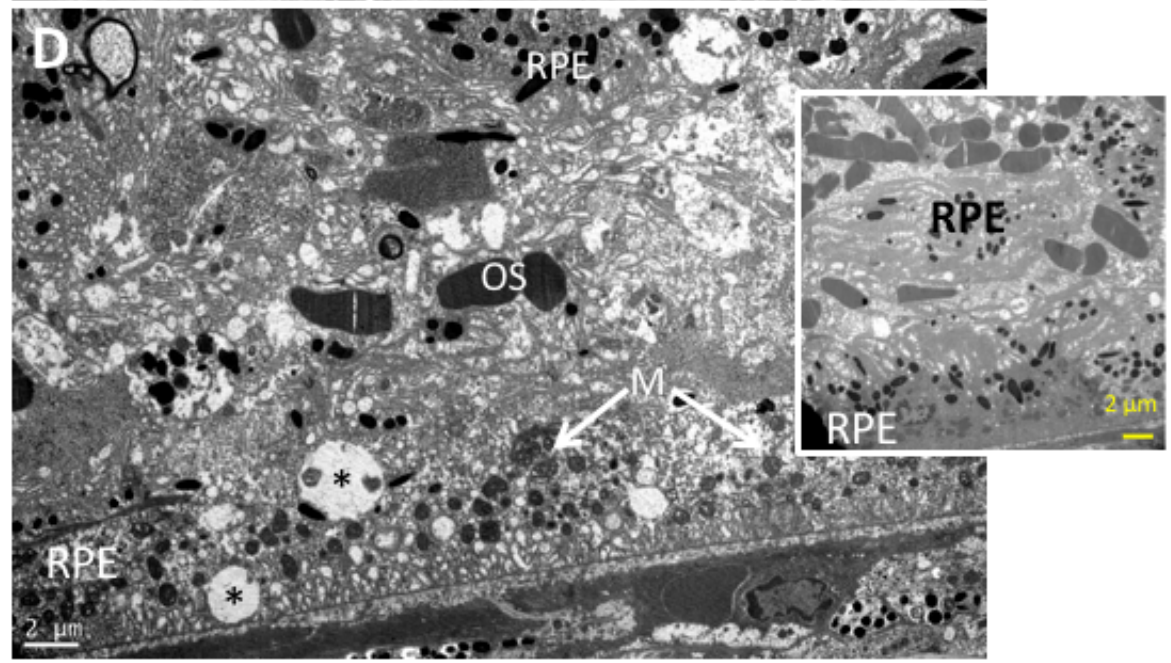
D
RPE
OS
M
*
*
RPE
2 µm
RPE
RPE
2 µm

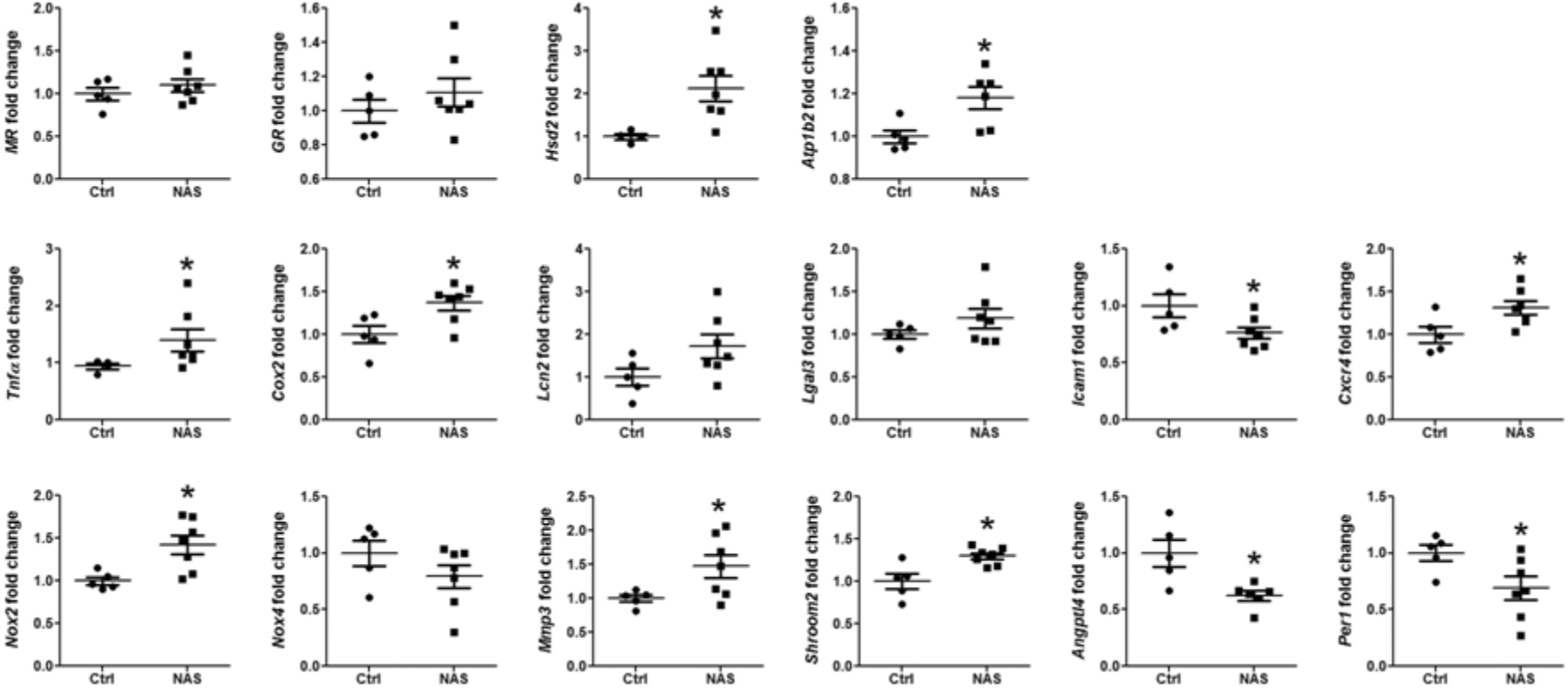
MR fold change
GR fold change
Hsd2 fold change
Atp1b2 fold change
Tnfα fold change
Cox2 fold change
Lcn2 fold change
Lgal3 fold change
Icam1 fold change
Cxcr4 fold change
Nox2 fold change
Nox4 fold change
Mmp3 fold change
Shroom2 fold change
Angptl4 fold change
Per1 fold change
Ctrl
NAS
*

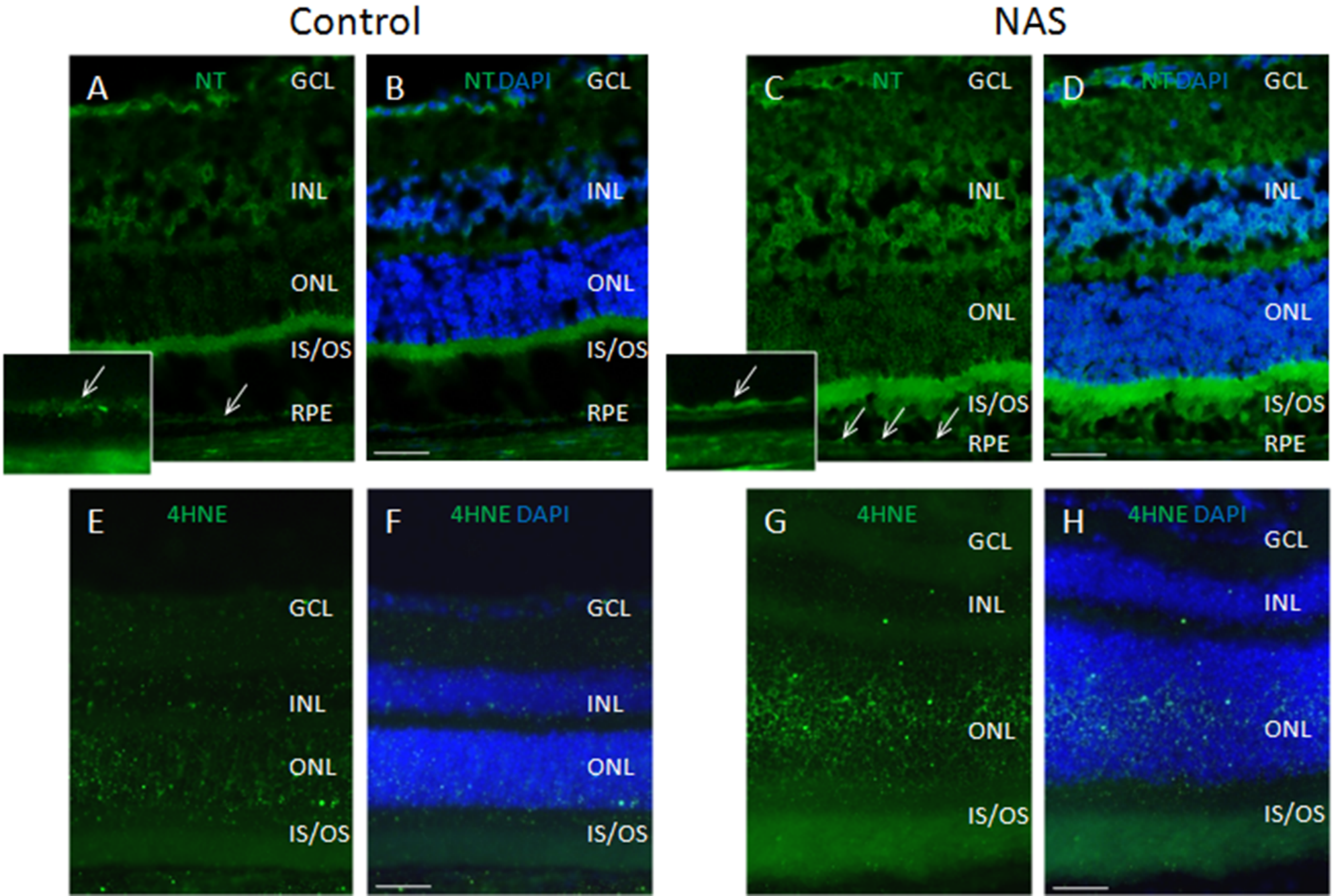
Control
NAS
A
NT
GCL
INL
ONL
IS/OS
RPE
B
NT DAPI
GCL
INL
ONL
IS/OS
RPE
C
NT
GCL
INL
ONL
IS/OS
RPE
D
NT DAPI
GCL
INL
ONL
IS/OS
RPE
E
4HNE
GCL
INL
ONL
IS/OS
F
4HNE DAPI
GCL
INL
ONL
IS/OS
G
4HNE
GCL
INL
ONL
IS/OS
H
4HNE DAPI
GCL
INL
ONL
IS/OS